

1
2
3
4
5
6

7 **Parallel genetic evolution and speciation from standing variation**

Commented [TA21]: I need to touch up
plot titles to make 'em consistent!

8
9 Ken A. Thompson^{1,2}, Matthew M. Osmond³ and Dolph Schluter²

10 ¹Corresponding author. Ken Thompson, email: kthomp1063@gmail.com

11 ²Biodiversity Research Centre and Department of Zoology, University of British Columbia,
12 Vancouver, Canada

13 ³Center for Population Biology, University of California, Davis, USA

14 Article type: Letter

15 Running title: Parallelism and speciation from standing variation

16 Keywords: Fisher's geometric model; ecological speciation; mutation-order speciation;
17 simulation; mathematical theory; convergent evolution; segregation variance; hybrid breakdown;
18 parallel evolution

19 Total word count: 5093

20 **Abstract** (289 Words)

21 Adaptation often proceeds via the sorting of standing variation, and natural selection acting on
22 pairs of populations is a quantitative continuum ranging from parallel to divergent. Yet, it is
23 unclear how the extent of parallel genetic evolution during adaptation from standing variation is
24 affected by the difference in the direction of selection between populations. Nor is it clear
25 whether the availability of standing variation for adaptation affects progress toward speciation in
26 a manner that depends on the difference in the direction of selection. We conducted a theoretical
27 study investigating these questions and have two primary findings. First, the extent of parallel
28 genetic evolution between two populations is expected to rapidly decline as the difference in
29 their directions of selection increases from fully parallel toward divergent, and this decline
30 occurs more rapidly in organisms with greater trait ‘dimensionality’. This rapid decline results
31 because seemingly small differences in the direction of selection cause steep reductions in the
32 fraction of alleles that are beneficial in both populations. For example, populations adapting to
33 optima separated by an angle of 33° have only 50% of potentially beneficial alleles in common
34 (for a case of five trait ‘dimensions’). Second, relative to when adaptation is from only new
35 mutation, adaptation from standing variation improves hybrid fitness under parallel selection and
36 reduces hybrid fitness under divergent selection. Under parallel selection, genetic parallelism
37 based on standing variation reduces the phenotypic segregation variance in hybrids, which
38 accordingly have high fitness in the parental environment. Under divergent selection, the
39 pleiotropic effects of alternative alleles fixed from standing variation lead to maladaptive
40 transgressive phenotypes when combined in hybrids. Adaptation from standing genetic variation
41 therefore slows progress toward speciation via parallel natural selection and facilitate progress
42 toward speciation via divergent natural selection.

43 **Impact summary** (262 words)

44 Much of adaptation, especially that which occurs rapidly, proceeds from the sorting of ancestral
45 standing variation rather than complete reliance on *de novo* mutation. In addition, evolutionary
46 biologists are increasingly embracing the fact that the difference in the direction of natural
47 selection on pairs of populations is a quantitative continuum ranging from completely parallel to
48 completely divergent. In this article, we ask two questions. First, how does the degree of genetic
49 parallelism—here, adaptation using the same alleles in allopatric populations—depend on the
50 differences in the direction of natural selection acting on two populations, from parallel (0°) to
51 divergent (180°)? And second, how does adaptation from standing variation affect progress
52 toward speciation, and does its effect depend on the direction of natural selection? We develop
53 theory to address these questions. We first find that very small differences in the direction of
54 selection (angle) can largely preclude genetic parallelism. Second, we find that adaptation from
55 standing variation has implications for speciation that change along the continuum from parallel
56 to divergent selection. Under parallel selection, high genetic parallelism causes inter-population
57 hybrids to have high mean fitness when their parents adapt from standing variation. As selection
58 tends toward divergent, adaptation from standing variation is less beneficial for hybrid fitness
59 and under completely divergent selection causes inter-population hybrids to have lower mean
60 fitness than when adaptation was from new mutation alone. In sum, our results provide general
61 insight into patterns of genetic parallelism and speciation along the continuum of parallel to
62 divergent natural selection when adaptation is from standing variation.

63 **Introduction**

64 In recent years, two general features of evolution by natural selection have become increasingly
65 established. First, adaptation often proceeds largely via the reassortment of ancestral standing
66 variation rather than via complete reliance on *de novo* mutations (Barrett and Schluter 2008).
67 And second, variation in the direction of natural selection acting on pairs of populations is best
68 represented by a quantitative continuum ranging from parallel selection—favouring identical
69 phenotypes—to divergent selection—favouring distinct phenotypes—rather than falling into
70 discrete ‘parallel’ or ‘divergent’ bins (Bolnick et al. 2018). It is unclear, however, how the extent
71 of parallel genetic evolution—use of the same alleles during adaptation—might depend on the
72 difference in the direction of selection experienced by a pair of populations. Whether or not
73 populations undergo parallel genetic evolution has consequences for the evolution of
74 reproductive isolating barriers between them (Schluter and Conte 2009). Yet, it is also unclear
75 whether adaptation from standing variation has implications for speciation that are distinct from
76 when adaptation is from new mutation alone, and whether its effect changes along the continuum
77 from parallel to divergent natural selection.

78 Adaptation facilitates progress towards speciation when populations evolve reproductive
79 isolating barriers as a by-product. One reason these reproductive isolating barriers might arise is
80 because genetic differences between populations have maladaptive consequences when
81 combined in hybrids (i.e., ‘postzygotic’ isolation), thereby reducing gene flow upon secondary
82 contact. When a pair of populations adapts in response to divergent natural selection, hybrids
83 might have a phenotype that is unfit in both parental environments (Schluter 2000). When a pair
84 of populations are subject to parallel selection, they may diverge genetically by chance (Mani
85 and Clarke 1990; Schluter 2009) and hybrids might have novel transgressive phenotypes that are

86 poorly suited to the common parental habitat (Barton 1989). Hybrid unfitness is therefore largely
87 determined by two factors. First, the hybrid phenotype distribution can ‘fall between the peaks’,
88 resulting from additive gene action and a maladaptive intermediate phenotype that is not adapted
89 to either parental environment (Hatfield and Schluter 1999). And second, cryptic genetic
90 divergence between parental populations can be released following hybridization and lead some
91 hybrids to possess novel and maladaptive transgressive phenotypes (Arnegard et al. 2014; Keagy
92 et al. 2016). How adaptation from standing variation affects progress toward speciation-by-
93 selection (Langerhans and Riesch 2013) is largely unexplored theoretically.

94 Adaptation from standing variation is common (Barrett and Schluter 2008) and underlies
95 some of the most spectacular adaptive radiations found in nature (Brawand et al. 2015). Genomic
96 studies in some systems also implicate standing variation as the major source of genetic
97 parallelism in replicate populations colonizing similar environments (Jones et al. 2012; Roesti et
98 al. 2014; Lee and Coop 2017). Previous research has shown that the correlation between
99 selection coefficients of a given allele in each of two populations inhabiting different
100 environments increases with the similarity in the direction of selection (equation 6 in Martin and
101 Lenormand 2015). Given this, we expected the extent of parallel genetic evolution for two
102 populations to decline from a maximum to a minimum value as the angle between the directions
103 of selection between them (θ) increases from completely parallel ($\theta = 0^\circ$) to completely
104 divergent ($\theta = 180^\circ$). Our specific goal was to characterize the pattern of decline in parallelism.
105 We also hypothesized that adaptation from standing variation would reduce the evolution of
106 reproductive isolation under parallel selection because parental populations would fix more of
107 the same alleles and therefore evolve fewer incompatibilities (Schluter 2009). Under divergent
108 selection we hypothesized that populations would fix alternative alleles regardless of whether

109 they were selected from standing variation or new mutation. Therefore, we expected standing
110 variation to have little effect on speciation by divergent selection compared to adaptation from
111 new mutation alone.

112 We conducted a theoretical investigation into parallel genetic evolution and speciation
113 from standing variation across the continuum from parallel to divergent natural selection. We
114 primarily used individual-based simulations and include some simple analytical arguments to
115 gain intuition. We compared results from simulations where adaptation proceeds simultaneously
116 via the sorting of ancestral standing genetic variation and *de novo* mutation to simulations where
117 adaptation proceeds via *de novo* mutation alone. Our results provide insight into the
118 circumstances under which we should expect high vs. low genetic parallelism and also suggest
119 that standing variation has substantial and unexpected implications for speciation that depend on
120 the difference in the direction of natural selection between populations.

121

122 **Methods**

123 We used computer simulations to investigate genetic parallelism and progress toward speciation
124 (via ecologically-dependent postzygotic reproductive isolation) from standing variation across
125 the continuum from parallel to divergent natural selection. Our simulations consider pairs of
126 populations and multivariate phenotypes determined by multiple additive loci. In our
127 simulations, a single ancestral population founds two identical populations that each adapt in
128 their respective environments without gene flow (i.e., allopatry; see Fig. 1A). After adaptation,
129 populations interbreed to form recombinant hybrids. This general colonization history—a single
130 population splitting into two populations that adapt to their respective novel environments in
131 allopatry—is modelled around the process of adaptation as it can occur in nature, for example in

132 postglacial fishes (Bell and Foster 1994) and in birds or plants isolated within glacial refugia
133 (e.g., Weir and Schlüter 2004; Pettengill and Moeller 2012). In many of these cases,
134 ecologically-dependent postzygotic isolation is thought to be essential for maintaining
135 reproductive isolation (Nosil 2012). See Table 1 for descriptions of all parameters and values
136 used in simulations (see **Data Accessibility** for information about accessing simulation code).

137

138 *Genotype to phenotype*

139 The phenotype of a haploid individual is represented by an m -dimensional vector, $\mathbf{z} = [z_1, z_2, \dots,$
140 $z_m]$, with m being the number of uncorrelated ‘traits’ or phenotypic ‘dimensions’ (for further
141 discussion of ‘dimensionality’, see Orr [2000] & Tenaillon [2014]). Each trait value, z_i , is
142 determined by the summed effects of alleles at all underlying loci (i.e., mutations act additively
143 to determine the phenotype), which are initially fixed for alleles with an effect of 0 on all m
144 traits. We present results from simulations with five phenotypic dimensions ($m = 5$) in the main
145 text, and results for alternative parameter combinations are found in the supplementary figures
146 (Figs. S1-S7).

147

148 *Life-cycle*

149 We model a Wright-Fisher population (Fisher 1930; Wright 1931) with haploid selection. Fitness
150 is a Gaussian function that depends on the Euclidean distance between an individual’s phenotype
151 and the phenotypic optimum, $\|\mathbf{z} - \mathbf{o}\|$, and the strength of selection, σ (e.g., Lande 1979):

$$152 W = \exp(-\sigma\|\mathbf{z} - \mathbf{o}\|^2/2) \quad (1)$$

153 N haploid parents are then randomly sampled with replacement from a multinomial distribution
154 with probabilities proportional to their fitness, W . Parents then randomly mate and produce two

155 haploid offspring per pair, with free recombination between all loci. With probability μ an
156 offspring gains a mutation; we assume an effectively infinite number of loci such that all
157 mutations arise at a previously unmutated locus ('infinite-sites' *sensu* Kimura [1969]).
158 Mutational effects are drawn from a multivariate normal distribution ('continuum-of-alleles'
159 *sensu* Kimura [1965]), with a mean of 0 and an SD of α in all m traits and no correlations among
160 traits (i.e., universal pleiotropy). Our qualitative conclusions are robust to alternative
161 assumptions about fitness functions (Fig. S8).

162

163 *Generating ancestral standing genetic variation*

164 We initiate two parental populations with standing genetic variation from a common ancestor
165 that adapt to novel phenotypic optima. To generate ancestral standing variation, we conducted
166 burn-in simulations of a large ancestral population ($N_{\text{anc}} = 10,000$) under stabilizing selection
167 ($\sigma_{\text{anc}} = 0.01$) at the origin ($\mathbf{o}_{\text{anc}} = [0, 0, \dots, 0]$) for 100,000 generations. All other parameters in the
168 ancestor (e.g., mutation rate) were identical to those of the pair of parental populations that it
169 founds. This parameter combination facilitates the accumulation of appreciable standing
170 variation (see Fig. S9), but we note that our general conclusions also hold if the ancestor is under
171 much stronger selection ($\sigma_{\text{anc}} = 1$) that puts it into the multivariate 'House-of-Cards' regime
172 (Turelli 1985; see Fig. S10).

173 Ancestral populations reached mutation-selection-drift balance such that the rate of
174 acquisition of new mutations was balanced by the rate of loss of mutations that arose in earlier
175 generations (Fig. S9A). Both the mean frequency of derived alleles and the phenotypic
176 (genotypic) variance were stable (Fig. S9B), as has been found in other models of phenotypes
177 under stabilizing selection (e.g., Barton 1989). Segregating derived alleles were all at unique loci

178 by assumption—that is, each polymorphic locus has exactly two alleles and each derived allele
179 can be traced back to a single mutation event. In addition, segregating derived alleles were at low
180 frequency in the ancestral population (see Fig. S9D for the site frequency spectrum). High
181 derived allele frequencies and fixation are sometimes reached by drift when mutations have
182 nearly-neutral selective coefficients and by positive selection when mutations compensate for
183 deleterious alleles that have risen to high frequency by drift (Hartl and Taubes 1996; Orr 2005).

184

185 *Adaptation to a new environment*

186 In simulations with standing genetic variation, a parental population was established by first
187 randomly choosing n polymorphic loci in the ancestor (see Fig. S11 for effect of n on genetic
188 parallelism and segregation variance). Each parental individual received the mutant (i.e.,
189 ‘derived’) allele at each of these n loci with a probability equal to the allele’s frequency in the
190 ancestor. Loci fixed in the ancestral population were also fixed in the parental population, but
191 were not considered when quantifying parallelism. This rather artificial sampling procedure
192 allowed us more control over the amount of standing genetic variation across simulations with
193 different parameter values (Figs. S1-S7). Further control was achieved by making the second
194 parental population initially identical to the first, so that each possessed the exact same collection
195 of genotypes and there were therefore no founder effects. Populations adapted from only new
196 (i.e., *de novo*) mutation when $n = 0$. Within each parameter combination, we began each
197 replicate simulation from a unique realization of the ancestor (i.e., distinct burn-in). After
198 initialization, parental populations adapted to their respective phenotypic optima without inter-
199 population gene flow (Fig. 1B), and adaptation proceeded via natural selection on ancestral
200 standing variation (if $n > 0$) and new mutation simultaneously.

201 Two properties of the new phenotypic optima are key. The first is the Euclidean distance
202 between each optimum and the origin, d (assumed the same for both parental populations for
203 simulations presented in main text). More distant optima yield a greater amount of genetic and
204 phenotypic change. In the main text we set $d = 1$, which is equivalent to 10 times the SD of
205 mutation effect size (α). The second key feature of the new optima is the angle of divergence, θ ,
206 separating vectors that originate at the origin and each pass through one of the parental optima
207 (dashed lines in Fig. 1B). Angle is used to quantify the difference in the direction of selection
208 from parallel ($\theta = 0^\circ$) to divergent ($\theta = 180^\circ$) and is explicitly invoked in most empirical metrics
209 that quantify phenotypic parallelism (see Bolnick et al. 2018). The value of θ is what determines
210 the mean phenotypic differences that evolve between parental populations in these simulations
211 (because d is held constant).

212 We ended the adaptation phase of simulations after multiple generations (parameter T , T
213 = 2000 in the main text), at which time all populations had reached their phenotypic optima (Fig.
214 S12A) and mutation-selection-drift balance (Fig. S12B). An unavoidable and important effect of
215 standing variation is that it quickens adaptation because populations do not have to ‘wait’ for
216 beneficial alleles to arise (Barrett and Schluter 2008). In our model and others like it (e.g., Barton
217 2001 & Chevin et al. 2014), reproductive isolation evolves rapidly during the initial stages of
218 adaptation. After populations reach their respective phenotypic optima, genetic divergence
219 accumulates slowly at a rate proportional to the mutation rate (Barton 1989, 2001; Chevin et al.
220 2014). Therefore, our general conclusions reflect quasi-equilibrium conditions rather than
221 transient states and are unaffected by standing variation’s influence on the speed of adaptation.

223 *Quantification of genetic parallelism and hybrid segregation variance & fitness*

224 After the adaptation phase of simulations had ended, we calculated the proportion of alleles that
225 fixed in both populations (i.e., genetic parallelism). We then paired random individuals from the
226 two parental populations to produce 100 recombinant haploid F₁ hybrids. Parents were sampled
227 without replacement such that each could contribute to a maximum of one mating. In the
228 hybrids, we quantified the phenotypic segregation variance and the relative mean fitness
229 compared to parents.

230 To quantify parallel genetic evolution between parental populations, we first determined
231 the number of alleles that fixed in each population ($Nfix_{P1}$ & $Nfix_{P2}$) and the number of alleles
232 that fixed in both populations ($Nfix_{Both}$). We then calculated our metric of ‘genetic parallelism’
233 as:

234
$$(Nfix_{Both} / Nfix_{P1} + Nfix_{Both} / Nfix_{P2}) / 2 \quad (2)$$

235 Values of 1 indicate complete genetic parallelism (i.e., all alleles that fixed were fixed in both
236 populations) and values of 0 indicate complete genetic non-parallelism (i.e., no allele was fixed
237 in both populations). We use this metric because of its ease of interpretation and note that it is
238 highly correlated with other metrics of genetic divergence between populations (e.g., FST; Fig.
239 S13).

240 After forming hybrids we quantified their phenotypic variation—the net segregation
241 variance (Wright 1968; Slatkin and Lande 1994)—calculated here as the mean phenotypic
242 variance across all m traits. We present analyses of individual axes of variance where relevant.
243 Higher segregation variance results when parents are differentiated by a greater number of
244 alternative alleles (holding effect size constant) or alleles of individually-larger effect (holding
245 number of alleles constant) (Castle 1921; Slatkin and Lande 1994; Chevin et al. 2014).

246 Segregation variance captures the phenotypic consequences of hybridization and has a direct
247 impact on fitness whereas genetic (non)parallelism is only indirectly related to fitness.
248 Phenotypic variance in parental populations before hybridization is near zero and does not differ
249 between populations founded with vs. without standing variation nor does it depend on the initial
250 distance to the optimum (d ; Fig. S12C).

251 An individual hybrid's fitness in a given parental environment was calculated from its
252 phenotype in the same manner as the fitness of parental populations (Fig. 1C). We determined
253 the fitness (equation 1) of each hybrid in both parental environments and recorded its fitness as
254 the larger of the two values. This can be imagined as, for example, giving the hybrid a choice of
255 alternative host-plants (Drès and Mallet 2002), where the choice is always for the host to which
256 it is better adapted. Our fitness metric reflects what is traditionally recognized as 'extrinsic'
257 postzygotic isolation (Coyne and Orr 2004), and explicitly considers environment-specific
258 epistasis for fitness (Bateson 1909; Dobzhansky 1937; Muller 1942; Chevin et al. 2014; Fraïsse
259 et al. 2016; see also Arnegard et al. 2014; Schumer et al. 2014; and Ono et al. 2017 for
260 discussion of environment-specific hybrid incompatibilities). We consider our model to be one
261 of 'extrinsic' rather than 'intrinsic' isolation because we do not consider traits such as 'gamete
262 viability or 'development' that have environment-independent (i.e., global) optima. Rather, traits
263 in our model are more akin to organism features like 'limb size' or 'beak depth', under
264 stabilizing selection with no global optimum. Because hybrids are recombinant, hybrid fitness
265 reflects both the effects of displacement of the mean phenotype from the optimum (the 'lag'
266 load) and what in diploids is known as 'hybrid breakdown' (Burton et al. 2006). We report
267 hybrid fitness relative to the parents for each individual simulation, calculated as: [mean fitness
268 of hybrids] / [mean fitness of parents].

269

270 **Results**

271 *Genetic parallelism and phenotypic segregation variance along the continuum from parallel to*
272 *divergent selection*

273 We first investigated how genetic parallelism between two populations—the fraction of alleles
274 that fixed in both populations vs. were unique to a single population—is associated with the
275 angle of divergence (θ) when adaptation is from standing variation (dark green line and points).
276 Genetic parallelism is highest under completely parallel natural selection ($\theta = 0^\circ$) and rapidly
277 decreases toward its minimum value as θ increases (Fig. 2A; see black line for visual comparison
278 of deviation from linearity). This rapid decrease in genetic parallelism also occurs when the
279 phenotypic distance *between* optima is used as the independent variable, although we note that
280 non-linearity is only appreciable in higher dimensions (see Fig. S14). There is considerable
281 variation in genetic parallelism even when populations adapt to identical environments, which
282 presumably results from stochastic processes in each run. For example, alleles are lost due to
283 drift, populations fix weakly deleterious alleles or different *de novo* mutations, and populations
284 fix alternative alleles from the standing variation early in the simulations which affects the
285 selection coefficients of all other alleles in later generations (Chevin and Hospital 2008). Genetic
286 parallelism never decreases to zero even under completely divergent selection ($\theta = 180^\circ$),
287 indicating that populations fix some deleterious alleles during the course of adaptation (although
288 genetic parallelism is nearer to zero in higher dimensions; Fig. S1-3). Our conclusion that genetic
289 parallelism rapidly decreases with θ are generally robust to variation in population size and
290 selection strength, except for when small populations are under weak selection (Fig. S1), likely

291 due to an overwhelming effect of drift (see Fig. S15 for divergence between populations due to
292 drift alone at various population sizes).

293 Genetic parallelism decreases with θ because the fraction of alleles that are beneficial in
294 each of the two populations declines as θ increases. For a given population, beneficial alleles
295 bring populations closer to the middle of a hypersphere centred at the phenotypic optimum
296 (Fisher 1930; see cartoon inset of Fig. 2B). Considering two populations, each with their own
297 hypersphere, a given allele is beneficial in both—and thus could fix in parallel via positive
298 natural selection—if it brings a population’s phenotype into the region where the two
299 hyperspheres overlap (purple region in Fig. 2B inset). The size of this *region of overlap*
300 decreases rapidly with θ (Fig. 2B; see Appendix for mathematical details), and therefore so does
301 the fraction of alleles present as standing variation that are beneficial in both populations. The
302 rate of decrease of overlap is faster with greater dimensionality (compare solid line to dashed
303 lines in Fig. 2B; see Figs. S1-S3 for confirmation with simulations in higher and lower
304 dimensions) but—perhaps surprisingly—does not depend on the distance to the optima (d ; if $d_1 =$
305 $d_2 = d$) and is not expected to change over the course of an ‘adaptive walk’ (*sensu* Orr [1998]; see
306 Appendix and Fig. A1 for detailed explanation). Briefly, this is because adaptation’s effect is to
307 shrink of the radii of the hyperspheres (at roughly equivalent rates in the two populations if
308 adaptation proceeds relatively deterministically). Thus, because the fraction of overlap (Eq. A1)
309 does not depend on the radii of the hyperspheres, the fraction of overlap is expected to remain
310 constant throughout adaptation.

311 It is possible to imagine an alternative case where θ is held constant, but populations
312 differ in the distance to their respective optima (i.e., different vector ‘lengths’ rather than ‘angles’
313 *sensu* Bolnick et al. [2018]). Even if selection acts in the exact same direction on two populations

314 ($\theta = 0^\circ$; $m = 5$), if the phenotypic optimum of population 2 is twice as far as that of population 1
315 from the ancestral phenotype, less than 5% of the alleles beneficial to population 2 are also
316 beneficial to population 1 (see Fig. S16). The region of overlap contains only small effect alleles,
317 however, which tend to be the sort of alleles that are present in the standing variation.

318 The changes in segregation variance generally mirror patterns of genetic parallelism (Fig.
319 2C). With standing variation, segregation variance is low under parallel selection and rapidly
320 increases with θ . Although Chevin et al. (2014) found that segregation variance (proportional to
321 their ‘variance load’) does not depend on θ , this is because their model did not permit genetic
322 parallelism. When there is no standing variation, segregation variance is not affected by the angle
323 of divergence (light green line and points in Fig. 2C; linear model $P > 0.9$ [as a check]), in
324 agreement with the findings of Chevin et al. (2014; their Fig. 2). At large angles, net segregation
325 variance is greater when populations adapt from standing variation than when they adapt from
326 new mutation alone, and the magnitude of this difference increases with dimensionality (see Fig.
327 S17). We explore the reasons for this below.

328

329 *Effect of standing variation on hybrid fitness across the continuum from parallel to divergent
330 selection*

331 In this section, we evaluate the effect of standing variation on hybrid fitness across the
332 continuum from parallel to divergent natural selection. The most readily observable pattern is
333 that the mean relative fitness of hybrids is lower under divergent selection than under parallel
334 selection regardless of whether adaptation proceeds with standing variation (Fig. 3A). This
335 pattern occurs mainly because the hybrid mean phenotype is increasingly distant from either

336 parental optimum as θ increases. In Fig. 3A, we plot the fitness of the hybrid mean phenotype
337 (the ‘lag’ load) as a thin black line.

338 Compared to when adaptation is from new mutation, adaptation from standing variation
339 improves mean hybrid fitness when parental populations adapt to similar optima but can reduce
340 hybrid fitness when parents undergo divergent adaptation (Fig. 3B). This pattern is caused by
341 environment-specific effects of segregation variance on mean hybrid fitness (Fig. 3C, Fig. 4).
342 When the hybrid phenotype distribution is centred at the phenotypic optimum, as it is under
343 parallel selection ($\theta = 0^\circ$), segregation variance is universally deleterious. When parental
344 populations adapt to identical optima from only new mutation, hybrids vary considerably around
345 the parental optimum and thus have relatively low fitness. When populations have access to a
346 common pool of standing variation, parallel genetic evolution leads to lower segregation
347 variance around the optimum and therefore higher mean fitness under parallel selection (Fig. 4A;
348 see Fig. S18 for similar results but for *maximum* hybrid fitness instead of mean).

349 At large angles of divergence, adaptation from standing variation reduces hybrid fitness
350 compared to when adaptation is from only new mutation—a result we did not anticipate. The
351 general reason for this is that hybrids (but not the parents) have reduced fitness in each parental
352 habitat as the angle of divergence increases, and some segregation variance is beneficial for
353 mean hybrid fitness when the mean hybrid phenotype is far from either optimum (see Fig. 3C).
354 This result is robust to variation in parameter values (see Figs. S4-S6), except for when selection
355 is very weak in small populations. We plot the distribution of hybrid phenotypes resulting from
356 representative simulations across the continuum from parallel to divergent selection in Figure 4.
357 From these figures, it is clear that there are appreciable differences in patterns of phenotypic
358 variation in hybrids when their parents adapt with standing variation vs. when adaptation is from

359 new mutation alone. Only phenotypic variation along the axis connecting parental optima (black
360 line connecting stars in Fig. 4) is beneficial, whereas variation along orthogonal axes is
361 deleterious. When $\theta = 180^\circ$, hybrids have reduced variation along the axis connecting parental
362 optima and slightly more variation along all other axes. Thus, maladaptive segregation variance
363 reduces hybrid fitness under large angles of divergence.

364 Why does adaptation from standing variation alter patterns of phenotypic segregation
365 variance in hybrids? As discussed above, adaptation from standing genetic variation reduces
366 segregation variance under parallel selection because parents fix the same alleles that therefore
367 do not segregate in hybrids. Populations adapting from standing variation also fix a greater
368 number of smaller effect alleles than simulations initiated without standing variation (Fig. 5A &
369 B), which contributes to the reduction in hybrid segregation variance along the mean axis of
370 selection in parents (average of dashed and blue lines in Fig. 4). Fixation of smaller-effect alleles
371 likely occurs under adaptation from standing variation because stabilizing selection removes
372 large-effect alleles from the standing variation (Fig. S9) and because weakly beneficial alleles
373 have a higher probability of fixation when present in standing variation compared to if they arose
374 *de novo* (Orr and Betancourt 2001; Hermisson and Pennings 2005; Matuszewski et al. 2015).
375 This latter effect seemed to allow alleles with more deleterious pleiotropic effects to fix during
376 adaptation from standing variation than when adaptation was from new mutation alone (Fig. 5C).
377 That is, populations initiated with standing genetic variation used a greater number of alleles—
378 each tending to have pleiotropic side-effects—to adapt to their new optimum. We quantified
379 pleiotropy by taking the ratio of the mean effect size of fixed alleles along the axis of selection in
380 parents (red or blue dashed lines in Fig 4) vs. the mean effect size across all orthogonal axes,
381 termed the ‘efficiency index’. Values of 1 (horizontal line in Fig. 5C) imply that an allele had an

382 equivalent effect along the axis of selection as on any orthogonal axis. Increasingly positive
383 values reflect alleles that take a population to the optimum more ‘efficiently’ (i.e., directly along
384 the dashed blue or red line in Fig. 4). Together, these results indicate that adaptive walks from
385 standing variation in our simulations involved more—slightly smaller—steps and are more
386 ‘meandering’ than adaptive walks from new mutation alone, which use fewer, slightly larger, and
387 more direct steps (but see Ralph and Coop 2015). These differences in the properties of alleles
388 fixed in simulations initiated with vs. without standing variation contribute to the patterns of
389 phenotypic segregation variance that influence mean hybrid fitness.

390

391 **Discussion**

392 In this study we investigated parallel genetic evolution and progress toward speciation under
393 adaptation from standing variation. Using a combination of individual-based simulations and
394 analytical models, we characterized how the extent of genetic parallelism from standing variation
395 changes with the angle of divergence. We then illustrated how adaptation from standing variation
396 affects hybrid fitness across the continuum from parallel to divergent natural selection, compared
397 to when adaptation is from only new mutation. Here, we highlight our key findings, predictions
398 for empirical systems, and discuss suggestions for future work.

399

400 *Key predictions and possible tests*

401 The first principal finding of our study is that the degree of genetic parallelism rapidly declines
402 as the angle of divergence increases from parallel toward divergent, especially when a large
403 number of traits affect fitness. Practically, this means that the extent of genetic parallelism also
404 declines quickly with phenotypic divergence. It is possible to test this prediction in natural or

405 experimental populations using techniques such as ‘Phenotypic Change Vector Analysis
406 (PCVA)’, which estimates important parameters such as the angle between the vectors and/or the
407 difference in their magnitudes (Bolnick et al. 2018). For example, hundreds of populations of
408 threespine stickleback (*Gasterosteus aculeatus*) have adapted to freshwater lakes and streams
409 from a shared marine ancestor (Jones et al. 2012). Appreciable phenotypic differences exist
410 among freshwater-adapted populations (Bell and Foster 1994), and if we assume that marine
411 populations represent the ‘ancestral’ state that founded ‘derived’ freshwater populations (see
412 Morris et al. 2018 for analysis of regional variation of the ‘contemporary ancestor’), parameter
413 estimates of marine-freshwater divergence from PCVA will give some indication about what the
414 genetic parallelism underlying marine-freshwater divergence is expected to be. Of course,
415 phenotypic measurements are imperfect and typically non-comprehensive, and accordingly any
416 estimates of **angle** and/or **distance** are necessarily made with some amount of error. Other cases
417 with repeated instances of easily-quantified phenotypic divergence (see Oke et al. 2017; Stuart et
418 al. 2017) are also amenable to this approach. Given that phenotypic and genetic parallelism are
419 not linearly related (Fig. S14), we suggest that analytical predictions about the extent of genetic
420 parallelism ought to be considered when generating predictions for empirical systems.

421 Our second principal finding is that—relative to when adaptation is from only *de novo*
422 mutation—adaptation from standing genetic variation improves the mean fitness of hybrids
423 under parallel natural selection, has little effect at intermediate angles of divergence, and reduces
424 mean hybrid fitness under completely divergent selection. Practically, this indicates that
425 adaptation from standing variation works against ‘mutation-order’ speciation and facilitates
426 ‘ecological’ speciation (Schluter 2009; Schluter and Conte 2009). This hypothesis could be
427 tested most readily in experimental systems where the amount of ancestral standing variation can

428 be easily manipulated, and where interpopulation hybrids can easily be generated to have their
429 fitness measured in parental environments.

430 We also emphasize that the mechanism through which adaptation from standing variation
431 affects fitness (relative to adaptation from *de novo* mutation) differs between simulations where
432 populations adapted under parallel vs. divergent selection. Under parallel selection, standing
433 variation's effect on hybrid fitness is caused by parallel genetic evolution and therefore
434 adaptation from standing variation is most likely to have an effect if populations adapting in
435 parallel start with *the same* standing variation. Under divergent selection, standing variation's
436 effect on hybrid fitness is not caused by genetic parallelism but rather on the characteristics of
437 adaptive walks from standing variation (more, meandering, and smaller steps). Therefore, our
438 predictions about the effect of adaptation from standing variation on hybrid fitness under
439 divergent selection should hold *regardless* of whether populations have the same or different
440 initial standing variation.

441

442 *Alternative sources of standing variation*

443 Our model addresses the case of adaptation from a pool of standing genetic variation at
444 mutation-selection-drift balance. This framework does not address cases of adaptation where
445 standing variation is generated from other sources. For example, in threespine stickleback, the
446 marine ancestral form is thought to maintain standing variation for freshwater-adapted alleles in
447 a balance between migration of alleles from freshwater populations and negative selection in the
448 sea (the 'transporter' hypothesis; Schluter and Conte 2009; Nelson and Cresko 2018). In this case,
449 the pool of standing variation is enriched for alleles that have already swept to fixation in
450 freshwater populations—that is, they are 'pre-tested' by selection—which might occur in linked

451 blocks of freshwater-adapted alleles in the sea. Scenarios such as this are especially likely to
452 cause genetic parallelism, more than is predicted from sort of standing variation modeled here
453 (Schluter and Conte 2009). The extent to which adaptation from standing variation proceeds via
454 the sorting of ‘naïve’ vs ‘pre-tested’ alleles is unresolved.

455

456 *Possible extensions*

457 Our study represents a step towards characterizing changes in genetic parallelism and progress
458 toward speciation in pairs of populations experiencing a variety of differences in the direction of
459 natural selection between them. Many of our assumptions—for example a lack of recurrent *de*
460 *novo* mutation or gene flow—reduce the extent of genetic parallelism (Nosil and Flaxman 2011;
461 Anderson and Harmon 2014; Ralph and Coop 2015). We also assumed universal pleiotropy and
462 it would be valuable to extend our approach to incorporate modularity. In addition, we
463 considered only haploid selection, no dominance, and strict additivity of allelic effects on
464 phenotypes (i.e., no epistasis). We also assumed that the sole fitness optima available to hybrids
465 are those that the two parents are adapted to (see Rieseberg et al. 1999). Our analytical results
466 consider only the fraction of mutations that are mutually beneficial, ignoring differences in the
467 probability that particular mutations arise and fix. Extending our approach to integrate the
468 distribution of fitness effects of new mutations (Eyre-Walker and Keightley 2007), the
469 correlation of selection coefficients across environments (Kassen 2014; Martin and Lenormand
470 2015), and existing theory on the probability of genetic parallelism from standing variation
471 (MacPherson and Nuismer 2017) will be valuable.

472 We also note that the only reproductive isolating barrier we considered was environment-
473 specific post-zygotic isolation. Post-zygotic isolation can also be environment-independent, and

474 such ‘intrinsic’ isolating barriers are correlated with genetic divergence between populations
475 (Orr 1995; Matute et al. 2010; Moyle and Nakazato 2010; Wang et al. 2015). Chevin et al.
476 (2014) quantified the strength of intrinsic postzygotic isolation using a metric of ‘variance load’,
477 which is proportional to our metric of net segregation variance. Therefore, our measure of
478 segregation variance might be interpreted as being proportional to the strength of intrinsic
479 barriers. We also did not consider pre-zygotic barriers such as assortative mating (Gavrilets
480 2004), which are also important for maintaining reproductive isolation. Accordingly, our results
481 might be most relevant for empirical systems where ecology-based postzygotic isolation has a
482 primary role in the origin of species.

483

484 *Concluding remarks*

485 In this study we characterized patterns of genetic parallelism and progress toward speciation
486 from standing variation in pairs of populations with quantitative differences in the direction of
487 selection between them. Our findings generate new hypotheses for empirical studies on genetic
488 parallelism and speciation. As evolutionary biologists develop increasingly powerful tools for
489 detecting parallel genetic adaptation in nature, it will be important to keep in mind that genetic
490 parallelism may be less common than we might intuit from patterns of selection and phenotypic
491 similarity. We have also shown that adaptation from standing variation is expected to weaken the
492 strength of isolating barriers that evolve between populations subject to parallel natural selection.
493 By contrast, our simulations indicate that adaptation from standing variation can actually
494 facilitate the process of speciation via divergent natural selection (i.e., ‘ecological’ speciation),
495 suggesting that adaptation from standing variation might have a role in adaptive radiation beyond
496 simply making it progress more quickly.

497

498 **Acknowledgements**

499 Discussions with S. Otto motivated and refined the approach used in this study. Feedback from
500 S. Arnold, M. Chapuisat, L. Chavarie, R. Holzman, A. MacPherson, S. Otto, L. Rieseberg, J.
501 Rolland, M. Urquhart-Cronish, R. Yamaguchi and three anonymous reviewers improved the
502 manuscript and/or reduced the demand for electricity by our simulations. K.A.T. was funded by
503 The University of British Columbia, the Natural Sciences and Engineering Research Council of
504 Canada (NSERC) and the Izaak Walton Killam Memorial Fund for Advanced Studies. M.M.O.
505 was funded by The University of British Columbia. D.S. was funded by the Canada Foundation
506 for Innovation, Genome BC, and NSERC.

507

508 **Author contributions**

509 K.A.T. and D.S. developed the original ideas upon which the paper is based. K.A.T. wrote the
510 first draft of the manuscript with input from M.M.O. and D.S., and all authors contributed to
511 subsequent revisions. M.M.O. wrote the simulations and supplied analytical derivations with
512 input from K.A.T. The simulations were performed by K.A.T. with input from M.M.O., and
513 K.A.T. processed, plotted, and analyzed the data.

514

515 **Data accessibility**

516 Python (version 3.6.4) scripts and resulting data, R (version 3.4.1) scripts to process and plot the
517 simulated data, and a Mathematica notebook (version 9; and PDF copy) to derive analytical
518 results will be archived on Dryad. For now, these are hosted on GitHub (<https://github.com/Ken->
519 A-Thompson/SVS).

520 **References**

- 521 Abramowitz, M., and I. A. Stegun. 1972. Handbook of mathematical functions: with formulas,
522 graphs, and mathematical tables. United States Department of Commerce, Washington DC,
523 USA.
- 524 Anderson, C. J. R., and L. Harmon. 2014. Ecological and mutation-order speciation in digital
525 organisms. *Am. Nat.* 183:257–268.
- 526 Arnegard, M. E., M. D. McGee, B. Matthews, K. B. Marchinko, G. L. Conte, S. Kabir, N.
527 Bedford, S. Bergek, Y. F. Chan, F. C. Jones, D. M. Kingsley, C. L. Peichel, and D. Schlüter.
528 2014. Genetics of ecological divergence during speciation. *Nature* 511:307–311.
- 529 Barrett, R. D. H., and D. Schlüter. 2008. Adaptation from standing genetic variation. *Trends
530 Ecol. Evol.* 23:38–44.
- 531 Barton, N. H. 1989. The divergence of a polygenic system subject to stabilizing selection,
532 mutation and drift. *Genet. Res.* 54:59–78.
- 533 Barton, N. H. 2001. The role of hybridization in evolution. *Mol. Ecol.* 10:551–568.
- 534 Bateson, W. 1909. Heredity and variation in modern lights. Pp. 85–101 *in* A. C. Seward, ed.
535 Darwin and Modern Science. Cambridge University Press, Cambridge.
- 536 Bell, M. A., and S. A. Foster. 1994. The evolutionary biology of the threespine stickleback.
537 Oxford University Press.
- 538 Bolnick, D. I., R. D. H. Barrett, K. B. Oke, D. J. Rennison, and Y. E. Stuart. 2018. (Non)Parallel
539 Evolution. *Annu. Rev. Ecol. Evol. Syst.* 49:303–330.
- 540 Brawand, D., C. E. Wagner, Y. I. Li, M. Malinsky, I. Keller, S. Fan, O. Simakov, A. Y. Ng, Z.
541 W. Lim, E. Bezault, J. Turner-Maier, J. Johnson, R. Alcazar, H. J. Noh, P. Russell, B. Aken,
542 J. Alföldi, C. Amemiya, N. Azzouzi, J. F. Baroiller, F. Barloy-Hubler, A. Berlin, R.

- 543 Bloomquist, K. L. Carleton, M. A. Conte, H. D'Cotta, O. Eshel, L. Gaffney, F. Galibert, H.
544 F. Gante, S. Gnerre, L. Greuter, R. Guyon, N. S. Haddad, W. Haerty, R. M. Harris, H. A.
545 Hofmann, T. Hourlier, G. Hulata, D. B. Jaffe, M. Lara, A. P. Lee, I. MacCallum, S.
546 Mwaiko, M. Nikaido, H. Nishihara, C. Ozouf-Costaz, D. J. Penman, D. Przybylski, M.
547 Rakotomanga, S. C. P. Renn, F. J. Ribeiro, M. Ron, W. Salzburger, L. Sanchez-Pulido, M.
548 E. Santos, S. Searle, T. Sharpe, R. Swofford, F. J. Tan, L. Williams, S. Young, S. Yin, N.
549 Okada, T. D. Kocher, E. A. Miska, E. S. Lander, B. Venkatesh, R. D. Fernald, A. Meyer, C.
550 P. Ponting, J. T. Streelman, K. Lindblad-Toh, O. Seehausen, and F. Di Palma. 2015. The
551 genomic substrate for adaptive radiation in African cichlid fish. *Nature* 513:375–381.
552 Burton, R. S., C. K. Ellison, and J. S. Harrison. 2006. The Sorry State of F 2 Hybrids:
553 Consequences of Rapid Mitochondrial DNA Evolution in Allopatric Populations. *Am. Nat.*
554 168:S14–S24.
555 Castle, W. E. 1921. An improved method of estimating the number of genetic factors concerned
556 in cases of blending inheritance. *Science* 54:223.
557 Chevin, L. M., G. Decorzent, and T. Lenormand. 2014. Niche dimensionality and the genetics of
558 ecological speciation. *Evolution* 68:1244–1256.
559 Chevin, L. M., and F. Hospital. 2008. Selective sweep at a quantitative trait locus in the presence
560 of background genetic variation. *Genetics* 180:1645–1660.
561 Coyne, J. A., and H. A. Orr. 2004. *Speciation*. Sinauer.
562 Dobzhansky, T. 1937. *Genetics and the origin of species*. Columbia University Press, New York.
563 Drès, M., and J. Mallet. 2002. Host races in plant-feeding insects and their importance in
564 sympatric speciation. *Philos. Trans. R. Soc. B Biol. Sci.* 357:471–492.
565 Eyre-Walker, A., and P. D. Keightley. 2007. The distribution of fitness effects of new mutations.

- 566 Nat. Rev. Genet. 8:610–618.
- 567 Fisher, R. F. 1930. The Genetical Theory of Natural Selection. Oxford University Press, Oxford,
568 UK.
- 569 Fraïsse, C., P. A. Gunnarsson, D. Roze, N. Bierne, and J. J. Welch. 2016. The genetics of
570 speciation: Insights from Fisher's geometric model. Evolution 70:1450–1464.
- 571 Gavrilets, S. 2004. Fitness Landscapes and the Origin of Species. Princeton University Press,
572 Princeton, NJ.
- 573 Hartl, D. L., and C. H. Taubes. 1996. Compensatory nearly neutral mutations: Selection without
574 adaptation. J. Theor. Biol. 182:303–309.
- 575 Hatfield, T., and D. Schlüter. 1999. Ecological speciation in sticklebacks: environment-
576 dependent hybrid fitness. Evolution 53:866–873.
- 577 Hermisson, J., and P. S. Pennings. 2005. Soft sweeps: Molecular population genetics of
578 adaptation from standing genetic variation. Genetics 169:2335–2352.
- 579 Hudson, R. R., M. Slatkin, and W. P. Maddison. 1992. Estimation of levels of gene flow from
580 DNA sequence data. Genetics 132:583–589.
- 581 Jones, F. C., M. G. Grabherr, Y. F. Chan, P. Russell, E. Mauceli, J. Johnson, R. Swofford, M.
582 Pirun, M. C. Zody, S. White, E. Birney, S. Searle, J. Schmutz, J. Grimwood, M. C. Dickson,
583 R. M. Myers, C. T. Miller, B. R. Summers, A. K. Knecht, S. D. Brady, H. Zhang, A. A.
584 Pollen, T. Howes, C. Amemiya, Broad Institute Genome Sequencing Platform & Whole
585 Genome Assembly Team, E. S. Lander, F. Di Palma, K. Lindblad-Toh, and D. M. Kingsley.
586 2012. The genomic basis of adaptive evolution in threespine sticklebacks. Nature 484:55–
587 61.
- 588 Kassen, R. 2014. Experimental evolution and the nature of biodiversity. Roberts.

- 589 Keagy, J., L. Lettieri, and J. W. Boughman. 2016. Male competition fitness landscapes predict
590 both forward and reverse speciation. *Ecol. Lett.* 19:71–80.
- 591 Kimura, M. 1965. A stochastic model concerning the maintenance of genetic variability in
592 quantitative characters. *Proc. Natl. Acad. Sci. U. S. A.* 54:731–736.
- 593 Kimura, M. 1969. The number of heterozygous nucleotide sites maintained in a finite population
594 due to steady flux of mutations. *Genetics* 61:893–903.
- 595 Lande, R. 1979. Quantitative genetic analysis of multivariate evolution, applied to brain: body
596 size allometry. *Evolution* 33:402–416.
- 597 Langerhans, R. B., and R. Riesch. 2013. Speciation by selection: A framework for understanding
598 ecology’s role in speciation. *Curr. Zool.* 59:31–52.
- 599 Lee, K. M., and G. Coop. 2017. Distinguishing among modes of convergent adaptation using
600 population genomic data. *Genetics* 207:1591–1619.
- 601 Li, S. 2011. Concise formulas for the area and volume of a hyperspherical cap. *Asian J. Math.*
602 *Stat.* 4:66–70.
- 603 MacPherson, A., and S. L. Nuismer. 2017. The probability of parallel genetic evolution from
604 standing genetic variation. *J. Evol. Biol.* 30:326–337.
- 605 Mani, G. S., and B. C. Clarke. 1990. Mutational order: A major atochastic process in evolution.
606 *Proc. R. Soc. B Biol. Sci.* 240:29–37.
- 607 Martin, G., and T. Lenormand. 2015. The fitness effect of mutations across environments:
608 Fisher’s geometrical model with multiple optima. *Evolution* 69:1433–1447.
- 609 Matuszewski, S., J. Hermisson, and M. Kopp. 2015. Catch me if you can: Adaptation from
610 standing genetic variation to a moving phenotypic optimum. *Genetics* 200:1255–1274.
- 611 Matute, D. R., I. A. Butler, D. A. Turissini, and J. A. Coyne. 2010. A Test of the Snowball

- 612 Theory for the Rate of Evolution of Hybrid Incompatibilities. *Source Sci. New Ser.*
613 329:1518–1521.
- 614 Morris, M. R. J., E. Bowles, B. E. Allen, H. A. Jamniczky, and S. M. Rogers. 2018.
615 Contemporary ancestor? Adaptive divergence from standing genetic variation in Pacific
616 marine threespine stickleback. *BMC Evol. Biol.* 18:113.
- 617 Moyle, L. C., and T. Nakazato. 2010. Hybrid incompatibility “snowballs” between *Solanum*
618 species. *Science* 329:1521–1523.
- 619 Muller, H. J. 1942. Isolating mechanisms, evolution and temperature. *Biol. Symp* 6:71–125.
- 620 Nei, M., and W.-H. Li. 1979. Mathematical model for studying genetic variation in terms of
621 restriction endonucleases. *Proc. Natl. Acad. Sci. U. S. A.* 76:5269–5273.
- 622 Nelson, T. C., and W. A. Cresko. 2018. Ancient genomic variation underlies repeated ecological
623 adaptation in young stickleback populations. *Evol. Lett.* 2:9–21.
- 624 Nosil, P. 2012. Ecological speciation. Oxford University Press, Oxford, UK.
- 625 Nosil, P., and S. M. Flaxman. 2011. Conditions for mutation-order speciation. *Proc. R. Soc. B*
626 *Biol. Sci.* 278:399–407.
- 627 Oke, K. B., G. Rolshausen, C. LeBlond, and A. P. Hendry. 2017. How parallel is parallel
628 evolution? A comparative analysis in fishes. *Am. Nat.* 190:1–16.
- 629 Ono, J., A. C. Gerstein, and S. P. Otto. 2017. Widespread genetic incompatibilities between first-
630 step mutations during parallel adaptation of *Saccharomyces cerevisiae* to a common
631 environment. *PLoS Biol.* 15:e1002591.
- 632 Orr, H. A. 2000. Adaptation and the cost of complexity. *Evolution* 54:13–20.
- 633 Orr, H. A. 2005. The genetic theory of adaptation: a brief history. *Nat. Rev. Genet.* 6:119–127.
- 634 Orr, H. A. 1998. The population genetics of adaptation: The distribution of factors fixed during

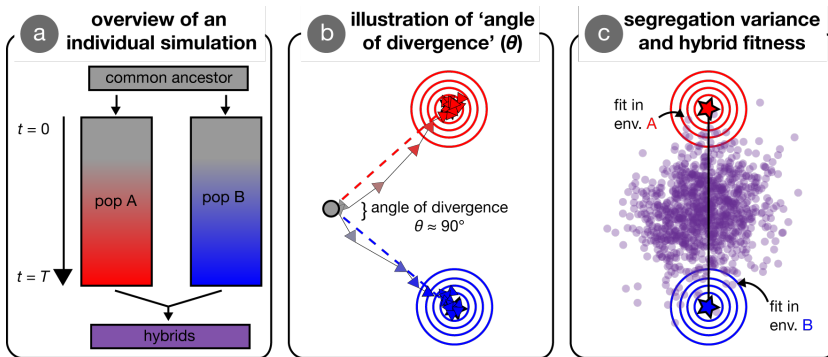
- 635 adaptive evolution. *Evolution* 52:935.
- 636 Orr, H. A. 1995. The population genetics of speciation: The evolution of hybrid
637 incompatibilities. *Genetics* 139:1805–1813.
- 638 Orr, H. A., and A. J. Betancourt. 2001. Haldane’s sieve and adaptation from the standing genetic
639 variation. *Genetics* 157:875–884.
- 640 Pettengill, J. B., and D. A. Moeller. 2012. Phylogeography of speciation: Allopatric divergence
641 and secondary contact between outcrossing and selfing *Clarkia*. *Mol. Ecol.* 21:4578–4592.
- 642 Ralph, P. L., and G. Coop. 2015. The Role of Standing Variation in Geographic Convergent
643 Adaptation. *Am. Nat.* 186:S5–S23.
- 644 Rieseberg, L. H., M. a Archer, and R. K. Wayne. 1999. Transgressive segregation, adaptation
645 and speciation. *Heredity* 83:363–372.
- 646 Roesti, M., S. Gavrilets, A. P. Hendry, W. Salzburger, and D. Berner. 2014. The genomic
647 signature of parallel adaptation from shared genetic variation. *Mol. Ecol.* 23:3944–3956.
- 648 Schlüter, D. 2009. Evidence for ecological speciation and its alternative. *Science* 323:737–741.
- 649 Schlüter, D. 2000. *The Ecology of Adaptive Radiation*. Oxford University Press, New York.
- 650 Schlüter, D., and G. L. Conte. 2009. Genetics and ecological speciation. *Proc. Natl. Acad. Sci.*
651 USA 106.Sup1:9955–62.
- 652 Schumer, M., R. Cui, D. L. Powell, R. Dresner, G. G. Rosenthal, and P. Andolfatto. 2014. High-
653 resolution mapping reveals hundreds of genetic incompatibilities in hybridizing fish species.
654 *Elife* 3:e02535.
- 655 Slatkin, M., and R. Lande. 1994. Segregation variance after hybridization of isolated
656 populations. *Genet. Res.* 64:51–56.
- 657 Stuart, Y. E., T. Veen, J. N. Weber, D. Hanson, M. Ravinet, B. K. Lohman, C. J. Thompson, T.

- 658 Tasneem, A. Doggett, R. Izen, N. Ahmed, R. D. H. Barrett, A. P. Hendry, C. L. Peichel, and
659 D. I. Bolnick. 2017. Contrasting effects of environment and genetics generate a continuum
660 of parallel evolution. *Nat. Ecol. Evol.* 1:0158.
- 661 Tenaillon, O. 2014. The utility of Fisher's geometric model in evolutionary genetics. *Annu. Rev.*
662 *Ecol. Evol. Syst.* 45:179–201.
- 663 Turelli, M. 1985. Effects of pleiotropy on predictions concerning mutation-selection balance for
664 polygenic traits. *Genetics* 111:165–195.
- 665 Turelli, M. 1984. Heritable genetic variation via mutation-selection balance: Lerch's zeta meets
666 the abdominal bristle. *Theor. Popul. Biol.* 25:138–193.
- 667 Wang, R. J., M. A. White, and B. A. Payseur. 2015. The Pace of hybrid incompatibility
668 evolution in house mice. *Genetics* 201:229–242.
- 669 Weir, J. T., and D. Schlüter. 2004. Ice sheets promote speciation in boreal birds. *Proc. R. Soc. B*
670 *Biol. Sci.* 271:1881–1887.
- 671 Wright, S. 1968. *Evolution and the Genetics of Populations Vol. 1. Genetic and Biometric*
672 *Foundations.* University of Chicago Press, Chicago, IL.
- 673 Wright, S. 1931. Evolution in mendelian populations. *Genetics* 16:97–159.
- 674

675 **Table 1.** Description of parameters and parameter values in parental populations for simulations
676 presented in the main text.

Parameter	Value
α , mutation size SD in each dimension	0.1
d , distance between ancestral and parental phenotypic optima	1
N , number of haploid individuals	1000
m , number of traits, or ‘dimensionality’	5
n , initial number of segregating loci	0 (new mutation only) or 100 (new mutation & standing genetic variation)
μ , probability an individual acquires a new mutation	0.001
σ , strength of selection	1
θ , angle of divergence (°)	$0 \leq \theta \leq 180$

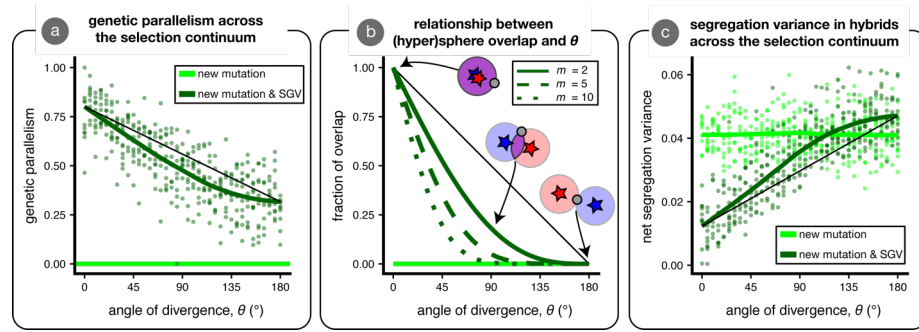
677



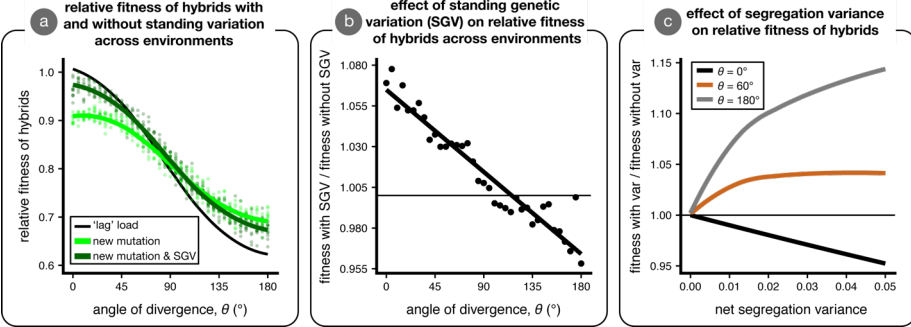
678

679 **Figure 1. Visual overview of simulations and concepts.** Panel (a) provides an overview of an
 680 individual simulation run. An ancestral population founds two initially-identical parental
 681 populations, that evolve independently for T generations in their respective environments. After
 682 T generations of adaptation, these parental populations interbreed to form hybrids. Panel (b)
 683 illustrates the process of adaptation in our simulations, wherein two populations (red and blue)
 684 arrows connect the mean phenotype every 200 generations) independently adapt to specified
 685 optima (red and blue stars; behind arrows in [b] but visible in [c]). Concentric circles represent
 686 fitness contours around the two optima. The ancestor state is indicated by the grey dot, with the
 687 angle of divergence, θ , shown between the two axes of selection (red and blue dashed lines;
 688 angle shown is approximately 90°). Panel (c) illustrates the segregation variance in a group of
 689 hybrids. Individual hybrids (purple points) that are near an optimum have high fitness when
 690 measured in that environment. The black line is the line connecting parental optima—variance
 691 along this line can increase mean hybrid fitness whereas variance orthogonal to this line is
 692 necessarily deleterious.

693

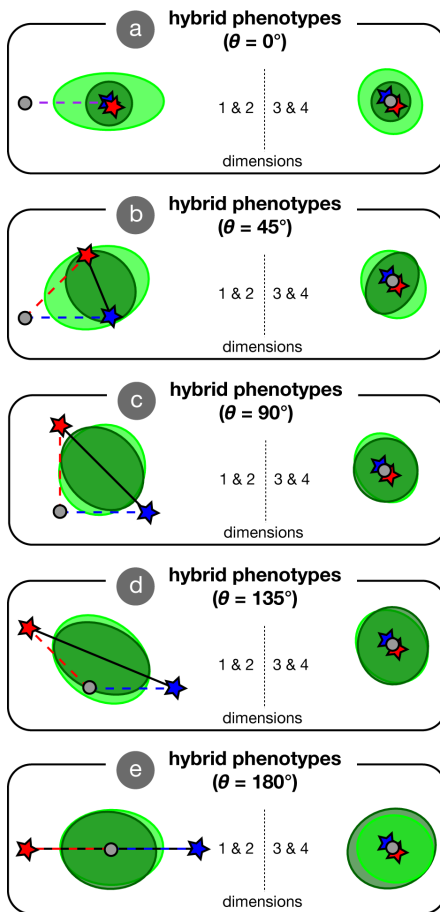


694 **Figure 2. Genetic parallelism and phenotypic segregation variance across the continuum**
 695 **from parallel to divergent natural selection.** We conducted 10 replicate simulations for optima
 696 separated by different angles ($\theta = 0^{\circ}$ to 180° ; $d = 1$). Parental populations adapted from either
 697 new mutation only ($n = 0$; light green) or from a combination of new mutation and standing
 698 genetic variation (SGV) ($n = 100$; dark green). Panel (a) shows the proportion of alleles that
 699 fixed in both populations (genetic parallelism; equation 2). Green lines are loess fits. The thin
 700 black line connects the fit at $\theta = 0^{\circ}$ to the fit at $\theta = 180^{\circ}$ and is shown to facilitate visualization of
 701 the nonlinearity. Panel (b) is an analytical result that depicts the relationship between θ and the
 702 fraction of overlap between two (hyper)spheres for three different dimensionalities (m) (see
 703 equation A1). In the inset cartoon, mutations that bring the phenotype into the red and blue
 704 regions are initially beneficial only in the ‘red’ or ‘blue’ environments, while mutations that bring
 705 the phenotype into the purple region are beneficial in both environments. The horizontal light
 706 green line is set at 0 where there is no overlap. Panel (c) shows the net phenotypic segregation
 707 variance in hybrids.



708

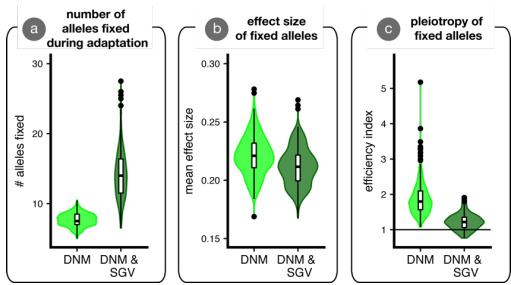
709 **Figure 3. The effect of standing variation on mean hybrid fitness across the continuum**
710 **from parallel to divergent natural selection.** Panel (a) shows the mean relative fitness of
711 hybrids—as compared to parents—across environments in simulations initiated without ($n = 0$;
712 light green) and with ($n = 100$; dark green) ancestral standing genetic variation. The thin black
713 line represents the mean relative fitness of hybrids due only to the deviation of the observed
714 mean phenotype from an optimum ('lag' load) and is close to 1 when the hybrid mean phenotype
715 is on the optimum. Panel (b) shows the effect of standing variation on mean relative hybrid
716 fitness (the ratio of values for dark / light green lines in panel [a]); the horizontal line indicates
717 no effect of standing variation on relative mean hybrid fitness. Panel (c) is an analytical result
718 that illustrates the relationship between segregation variance and mean hybrid fitness for three
719 angles of divergence (black, $\theta = 0^{\circ}$; brown, $\theta = 60^{\circ}$; grey, $\theta = 180^{\circ}$) when the hybrid phenotype
720 is multivariate normal with a mean exactly in between the two parental optima and equal
721 variance in all phenotypic dimensions (no covariance). Hybrid fitness is plotted for each angle
722 relative to the case of no variance; the horizontal line indicates when segregation variance has no
723 effect on hybrid fitness.



725 **Figure 4. The effect of standing variation on the distribution of hybrid phenotypes.** We plot
 726 an ellipse containing 95 % of hybrid phenotypes for five angles of divergence (θ) evenly spaced
 727 along the continuum of (a) completely parallel (0°) to completely (e) divergent (180°) selection
 728 for simulations where populations adapted from only new mutation (light green) or both new
 729 mutation and standing genetic variation (dark green). Each ellipse is fit to 1000 hybrids resulting
 730 from 10 replicate simulations. The left side of each panel shows the first two trait dimensions—

731 the only dimensions in which the optima might differ. The right side of each panel shows the
732 third and fourth dimensions—under stabilizing selection for panel depicts 100 hybrids from
733 each scenario from a single representative simulation run. (Parental optima are depicted as stars
734 and the origin (ancestral optimum) is shown as a grey dot. The axes of selection connect the
735 origin and optima (dashed red and blue lines) and we also show the axis connecting parental
736 optima as a black line. Ellipse plotting order is reversed on the right side of panel (e) to facilitate
737 visualization.

738



739

740 **Figure 5. Properties of alleles fixed during adaptation.** We show results from simulations
 741 where parental populations adapted from only *de novo* mutation (light green; DNM) vs.
 742 adaptation from standing variation and new mutation (dark green; DNM & SGV). Each replicate
 743 simulation contributed one data point to the plot. Panel (a) shows the average number of alleles
 744 fixed during adaptation. Panel (b) shows the average effect size (Euclidean length of mutation
 745 vector) of alleles fixed during adaptation. Panel (c) shows the allele ‘efficiency index’, which
 746 plots the ratio of a fixed mutations’ effect size in the direction of selection vs. orthogonal
 747 directions. Values of 1 are equally balanced in these directions, and mutations are more
 748 ‘efficient’ (i.e., they point more directly at the optimum) as this index increases. Statistical tests
 749 confirm all differences as highly significant (not shown).

750

751
752

Supporting information for:

753 Patterns of speciation and parallel genetic adaptation from standing variation

754 **by**

755 Ken A. Thompson, Matthew M. Osmond and Dolph Schlüter

756

757 **Contents:**

758 Appendix

759 Figures S1-18.

760

761 **Appendix**

762 Here we outline an explanation for why genetic parallelism decreases rapidly with the angle of
763 divergence, θ (Fig. 2A, and distance between optima (Fig. S15B). Our explanation focuses on
764 the extent of phenotypic space wherein mutations improve the fitness of both adapting
765 populations in their respective environments. At the time of founding both adapting populations
766 have the same mean phenotype, which is the mean ancestral phenotype. Mutations that move this
767 ancestral mean phenotype into the region that leads to higher fitness in both parental
768 environments are thus beneficial in both populations. The region of phenotypic space that has
769 higher fitness than the mean phenotype in one environment is a hypersphere (of dimension m),
770 centred on the optimum with a radius equal to the distance between the mean phenotype and the
771 optimum, d . A similar hypersphere characterizes the phenotypic space that has higher fitness
772 than the mean phenotype in the other parental environment. The region that is mutually
773 beneficial is then the intersection of two hyperspheres, which is the union of two hyperspherical
774 caps.

775 Fortunately, the volume of a hyperspherical cap is known for any dimension, m (Li
776 2011). It depends on the dimensionality (m), the radii of the two hyperspheres (d), and the
777 distance between their centers (δ). In our case the distance between the two centres is $\delta = 2d *$
778 $\sin(\theta/2)$. The amount of phenotypic space that is beneficial in a given environment is simply the
779 volume of one of the hyperspheres. Thus, dividing the volume of the mutually-beneficial space
780 (the union of the hyperspherical caps) by the volume of the space beneficial in a given
781 environment (one of the hyperspheres) gives the fraction of beneficial mutations which are
782 mutually beneficial. Using the formula given by Li (2011; their eqn 3) for the volume of a
783 hyperspherical cap created by the intersection of two m -dimensional hyperspheres with radii d

784 whose centres are distance $\delta = 2d * \sin(\theta/2)$ apart, the fraction of beneficial mutations that are
785 expected to be beneficial in both is:

786 $I_x[(1 + m)/2, 1/2]$ (A1)

787 where $I_x[a, b]$ is the regularized incomplete beta function (Equation 6.6.2 in Abramowitz and
788 Stegun [1972]) and here $x = \cos(\theta/2)^2$. Eq. A1 depends on only m and θ , that is the solution is
789 independent of the distance from the ancestor to the new optima, d . We refer to Eq. A1 as the
790 fraction of overlap in the main text, but note that this is only true when $d_1 = d_2$ (the formula is
791 more complex when $d_1 \neq d_2$, but can easily be used, e.g., Fig. S16B). The incomplete regularized
792 beta function arises from integrating $\sin^m(\theta)$ over θ (Li 2011).

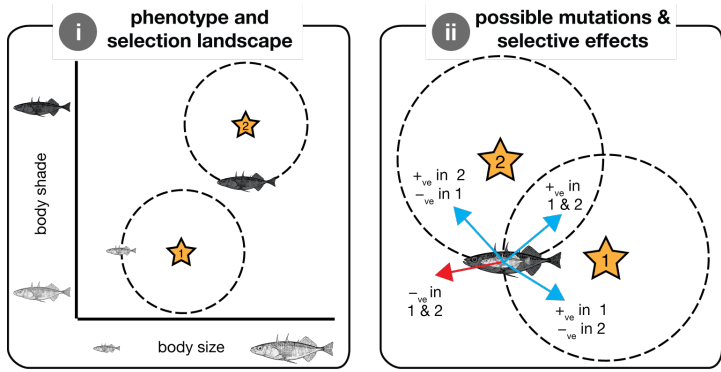
793 The solution of Eq. A1 exhibits a rapid decrease with θ for all values of $m > 0$, and the
794 decrease is faster for greater values of m (Fig. 2B). Thus, if standing genetic variation was
795 uniformly distributed throughout the beneficial hyperspheres, the percent of segregating
796 beneficial mutations that were beneficial in both parental populations, and thus expected to
797 potentially fix in both, would decrease rapidly with the angle of divergence.

798 The above analysis considers only the very onset of adaptation, when the two parental
799 populations have the same mean phenotypes, such that the fraction of phenotypic space that is
800 beneficial in one population that is also beneficial in the other population (call this X) is
801 equivalent to the fraction of possible beneficial mutations (if uniformly distributed across the
802 hyperspheres) that are beneficial in both populations (call this Y). As adaptation proceeds the
803 mean phenotypes of the parental populations depart from one another and X therefore no longer
804 equals Y . This is because mutations are vectors that move a phenotype in a particular direction,
805 and thus a mutually beneficial point in phenotypic space is only guaranteed to be a mutually
806 beneficial mutation if both populations have the same mean phenotype.

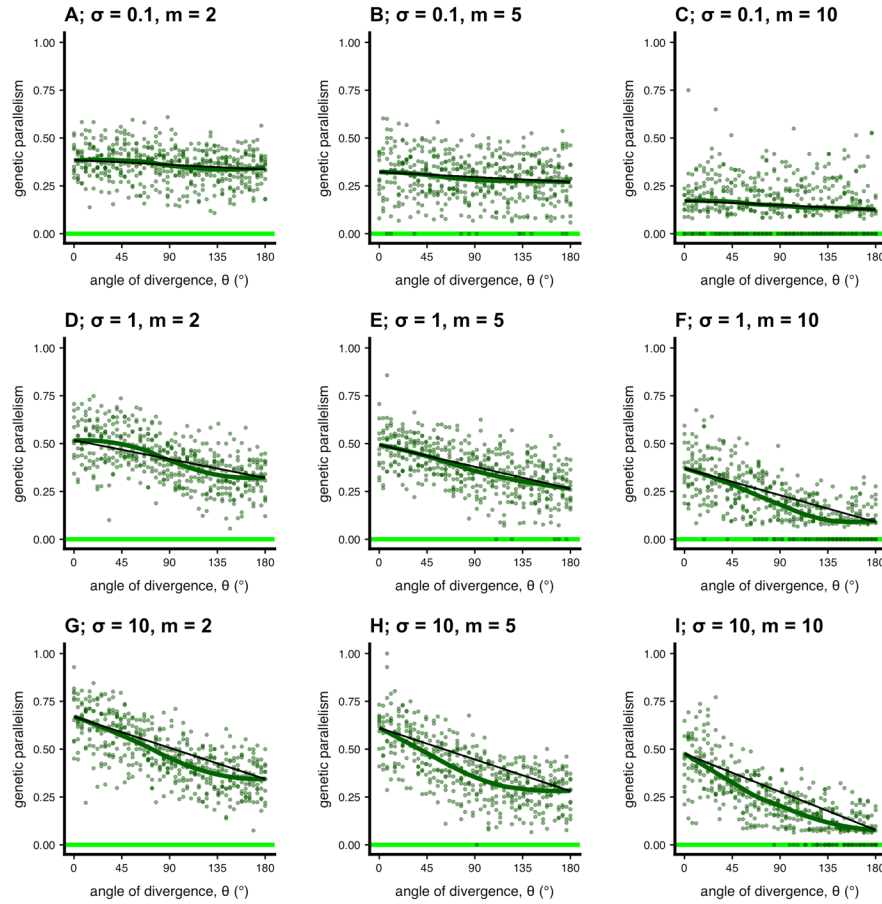
807 To account for the inequality between phenotypic space (X) and mutational vectors (Y)
808 during adaptation we must shift the mean phenotypes so that they are at the same point in
809 phenotypic space and move their optima by an identical translation (see Fig. A1). We then have
810 $X=Y$. One way to imagine this is to keep the mean phenotypes in place at the mean ancestral
811 phenotype (the origin) and consider adaptation as the movement of the optima closer to the mean
812 phenotypes. From this perspective, adaptation's effect is a shrinking of the radii of the
813 hyperspheres (at roughly equivalent rates in the two populations if adaptation proceeds relatively
814 deterministically). Thus, because the fraction of overlap (Eq. A1) does not depend on the radii of
815 the hyperspheres, the fraction of overlap is expected to remain constant throughout adaptation.

816 In reality and in our simulations, standing genetic variation is not uniformly distributed,
817 the probability of fixation varies across the region of overlap, and adaptation uses up some of the
818 standing variation so that the distribution of standing variation changes with time. Taking the
819 first two complications into account would require weighted averages across the space contained
820 in the hyperspherical caps, which is beyond the scope of our study. The third complication is yet
821 more involved and would require an analysis of how standing genetic variation is used as
822 adaptation proceeds (i.e., how the distribution of segregating effects and allele frequencies shift
823 as alleles fix). Such a calculation is also beyond the scope of this article. Despite these
824 complications, it seems as though the simple analysis above qualitatively captures the essence of
825 why genetic parallelism decreases rapidly with the angle of divergence.

826



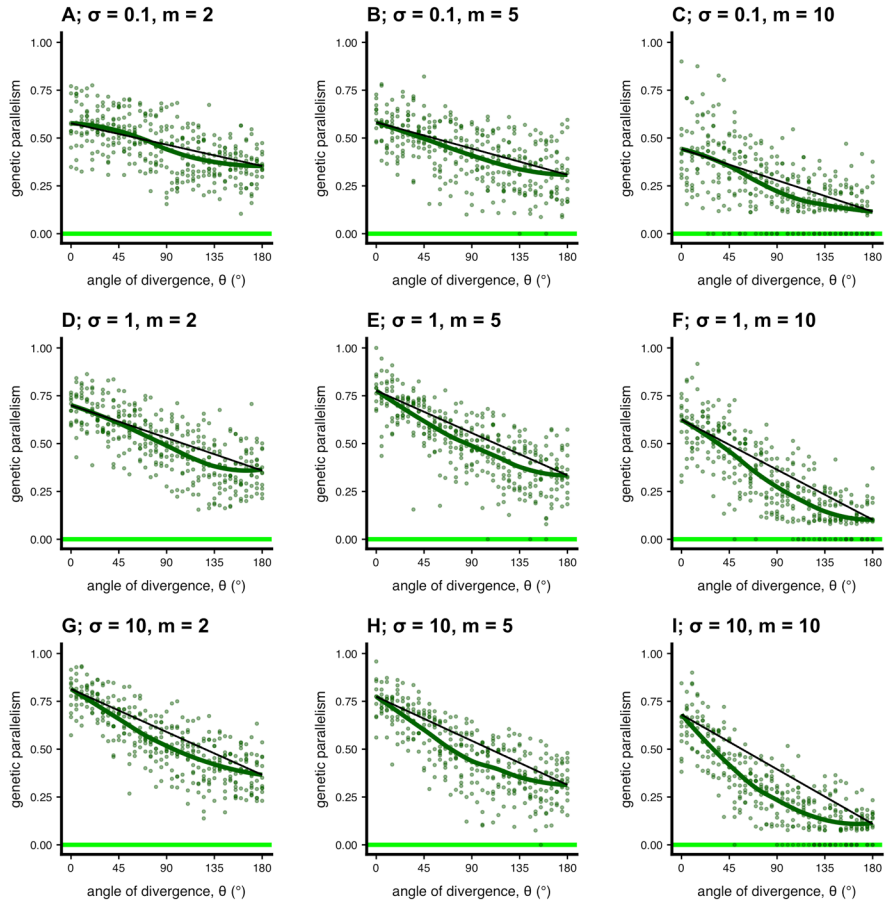
828 **Fig. A1. Cartoon illustration of why divergence among populations does not affect whether**
 829 **an allele is beneficial in both of them.** Panel (i) depicts the phenotype landscape and selection
 830 landscape. Variation in the horizontal dimension reflects phenotypic variation in body size, and
 831 the vertical dimension reflects variation in body shade. We depict two ‘populations’ with
 832 differences in body size and shade (small & light; big & dark). The stars reflect local optima
 833 after a hypothetical environmental shift—selection favours adaptation toward a larger body size
 834 in population 1 and selection for darker body shade in population 2. If we illustrate the circle of
 835 beneficial mutational space (dashed circles) with respect to the current phenotypic position they
 836 do not overlap. Panel (ii) illustrates the selection landscape as it is ‘experienced’ by each
 837 population. An allele that slightly increases body size and darkens the body shade from the
 838 current phenotype (the position of the fish cartoons) is beneficial (blue) in both of populations.
 839 Some alleles are beneficial in only one population, and others are deleterious in both (red). Thus,
 840 even though the spheres do not overlap in (i) it is not the case that they populations will undergo
 841 non-parallel genetic evolution.

842 **Supplementary figures**

843

844 **Figure S1. Genetic parallelism across the continuum of parallel to divergent natural**
 845 **selection (pop size = 100).** This figure presents simulations similar to Fig. 2A in the main text
 846 but with varying parameter values (selection [σ] and dimensionality [m]). We ran these particular
 847 simulations for $T = 5000$ generations. All other parameters as in main text.

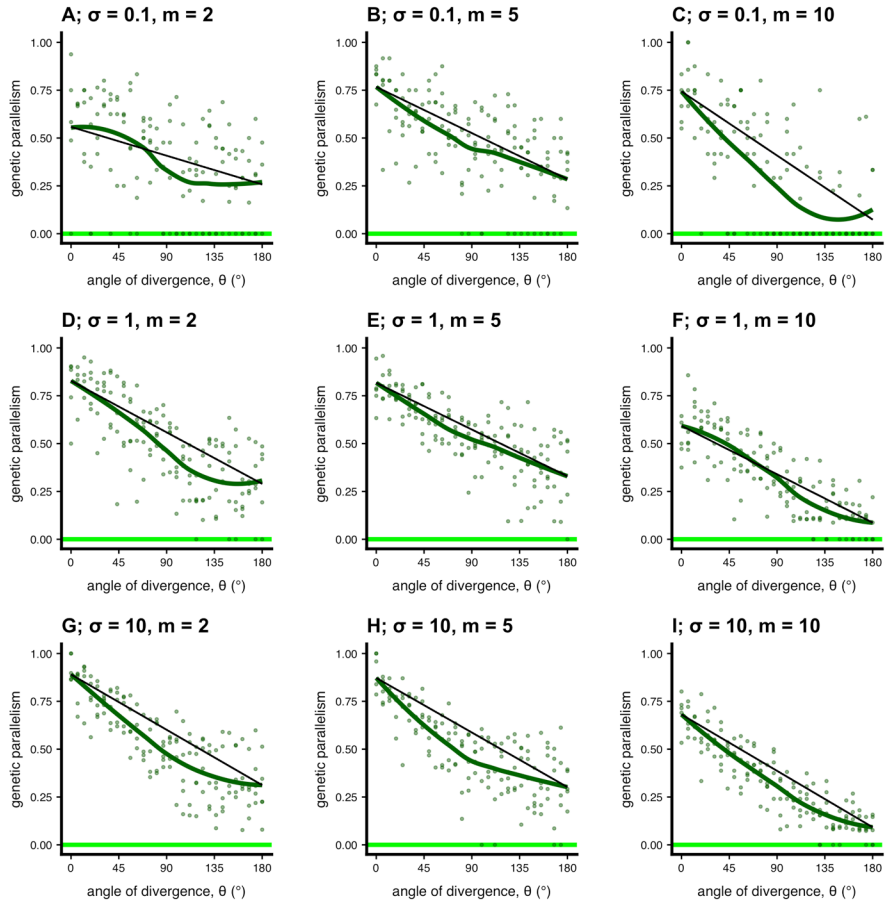
848



849

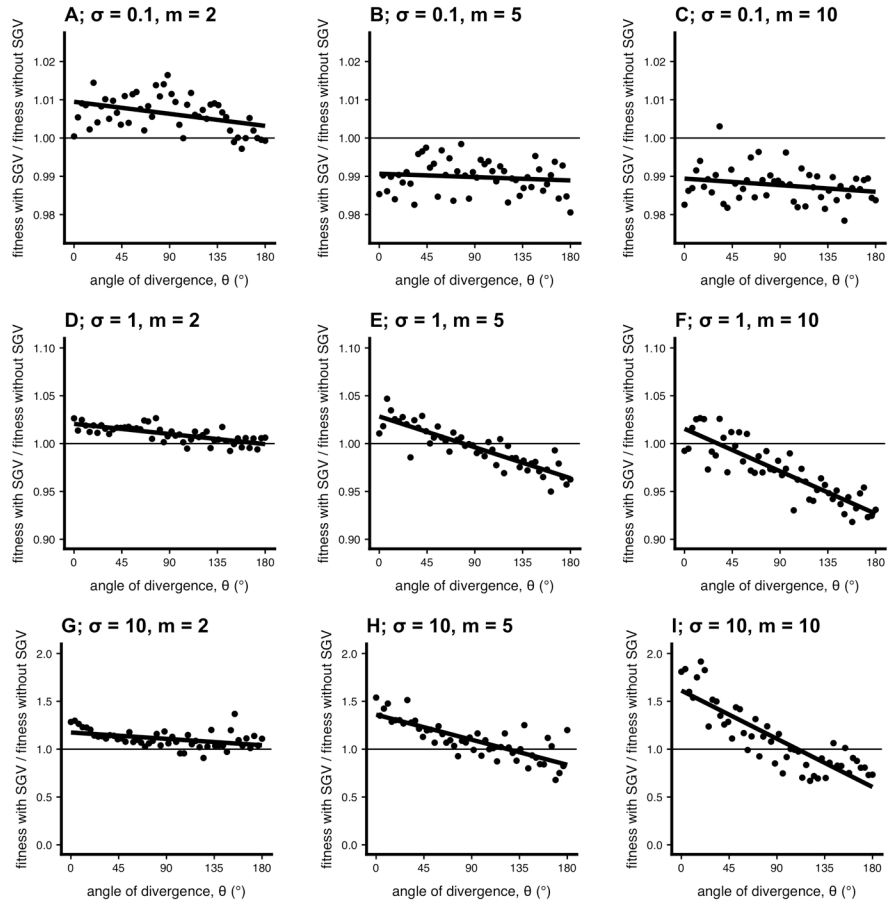
850

Figure S2. Genetic parallelism across the continuum of parallel to divergent natural selection (pop size = 1000). This figure presents simulations similar to Fig. 2A in the main text but with varying parameter values (selection [σ] and dimensionality [m]). We ran these particular simulations for $T = 2000$ generations. All other parameters as in main text.



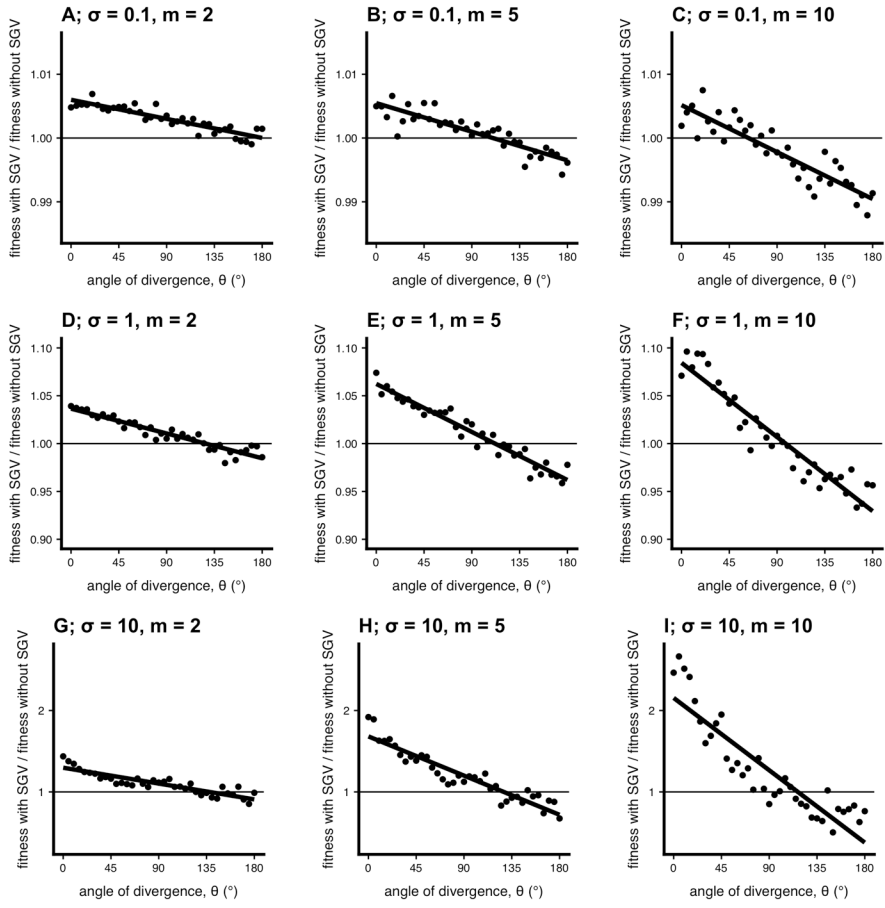
854

855 **Figure S3. Genetic parallelism across the continuum of parallel to divergent natural**
 856 **selection (pop size = 5000).** This figure presents simulations similar to Fig. 2A in the main text
 857 but with varying parameter values (selection [σ] and dimensionality [m]). We ran these particular
 858 simulations for $T = 1000$ generations. All other parameters as in main text. These simulations are
 859 computationally intensive and were therefore not run for as many replicates as those plotted in
 860 Fig. S2 or S3.



861
862
863
864
865
866
867

Figure S4. Effect of standing genetic variation on hybrid fitness the continuum of parallel to divergent natural selection (pop size = 100). This figure presents simulations similar to Fig. 3B in the main text but with varying parameter values (selection [σ] and dimensionality [m]). We ran these particular simulations for $T = 5000$ generations. All other parameters as in main text. Note different y-axis scales across rows.

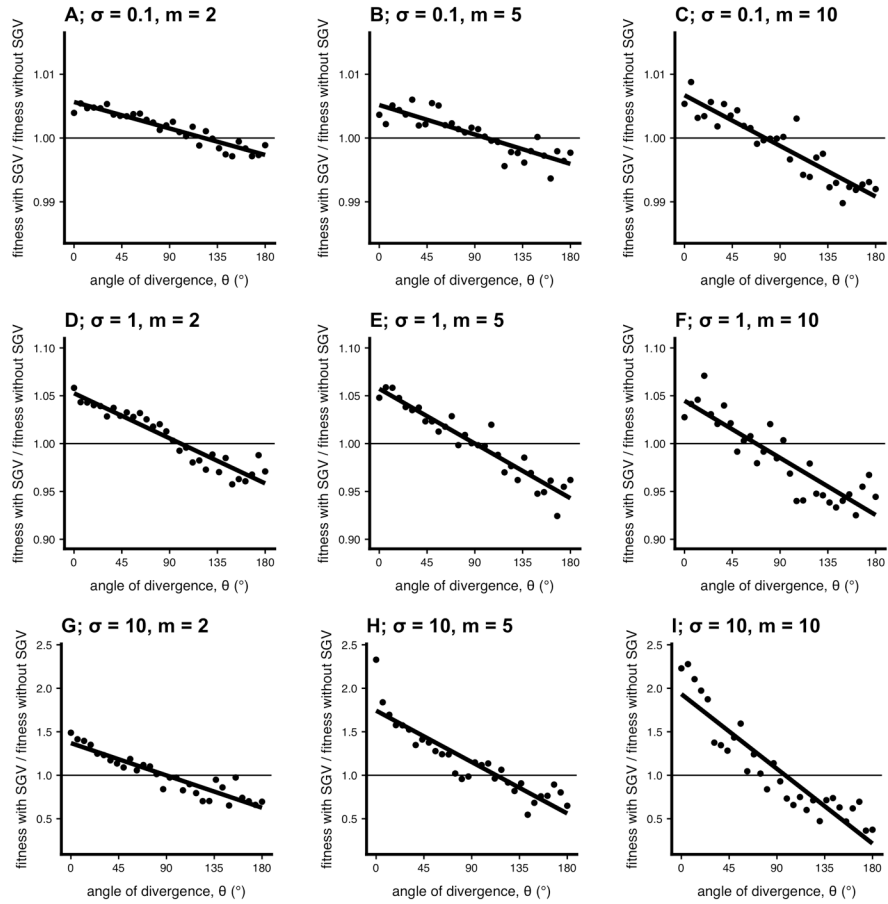


868

869

**Figure S5. Effect of standing genetic variation on hybrid fitness the continuum of parallel
870 to divergent natural selection (pop size = 1000).** This figure presents simulations similar to
871 Fig. 3B in the main text but with varying parameter values (selection [σ] and dimensionality
872 [m]). We ran these particular simulations for $T = 2000$ generations. All other parameters as in
873 main text. Note different y-axis scales across rows.

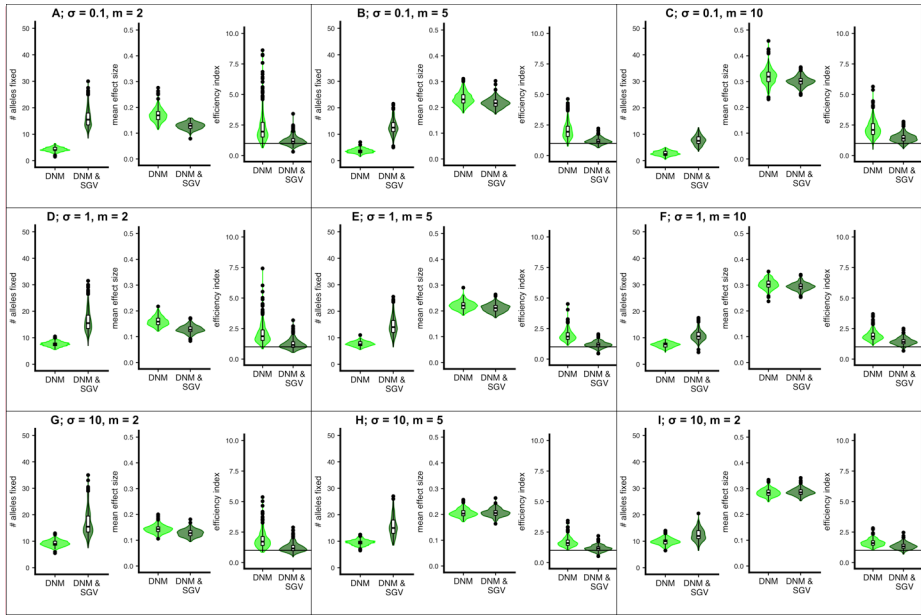
874



875

876 **Figure S6. Effect of standing genetic variation on hybrid fitness the continuum of parallel**
 877 **to divergent natural selection (pop size = 5000).** This figure presents simulations similar to
 878 Fig. 3B in the main text but with varying parameter values (selection [σ] and dimensionality
 879 [m]). We ran these particular simulations for $T = 1000$ generations. All other parameters as in
 880 main text. Note different y-axis scales across rows.

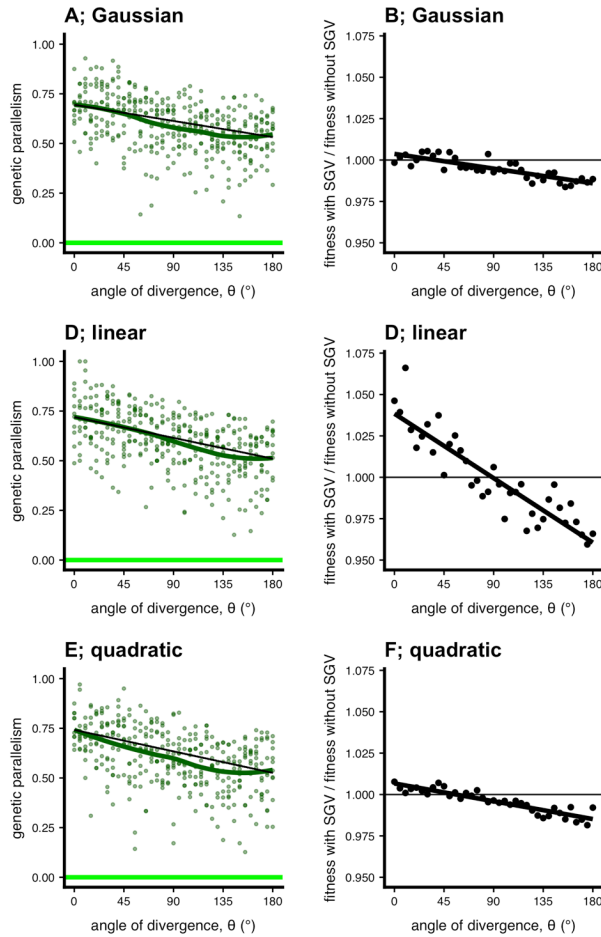
881



882
883
884
885
886
887

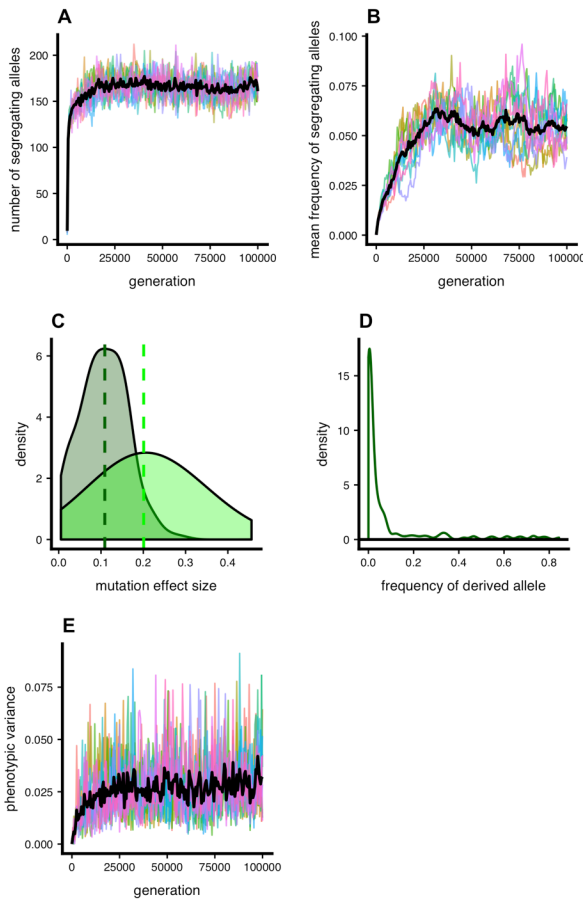
Figure S7. Properties of fixed mutations under a variety of parameter combinations ($N=1000$). This figure presents simulations similar to Fig. 5 in the main text but with varying parameter values (selection [σ] and dimensionality [m]). See main text and panel description of Fig. 5 for more detail. Patterns were similar for other population sizes.

Commented [TA22]: M = 2 error in bottom corner



888
889
890
891
892
893
894
895
896
897

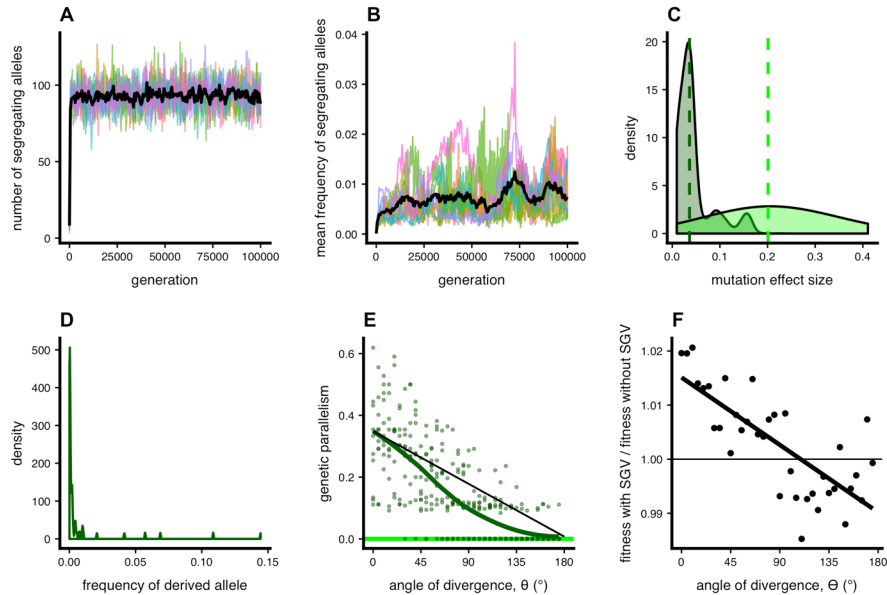
Figure S8. Simulations under various fitness functions. Here we plot simulations across environments for (A & B) Gaussian ($W = \exp(-\sigma \|z - \mathbf{o}\|^2/2)$; equation 1), (C & D) linear ($W = 1 - \sigma \|z - \mathbf{o}\|$), and (E & F) quadratic ($W = 1 - \sigma \|z - \mathbf{o}\|^2/2$) fitness functions. We show results for both genetic parallelism and the effect of standing variation on hybrid fitness. We ran these simulations with a nearer optimum and weaker selection ($d = 0.5$, $\sigma = 0.5$, $N = 1000$, $m = 5$) because populations otherwise became extinct with linear/quadratic fitness functions. Under these conditions, the non-linear decrease in parallelism is less substantial for all parameter values. Nevertheless, the patterns are qualitatively similar among the three sets of simulations (note differences in y-axis scales).



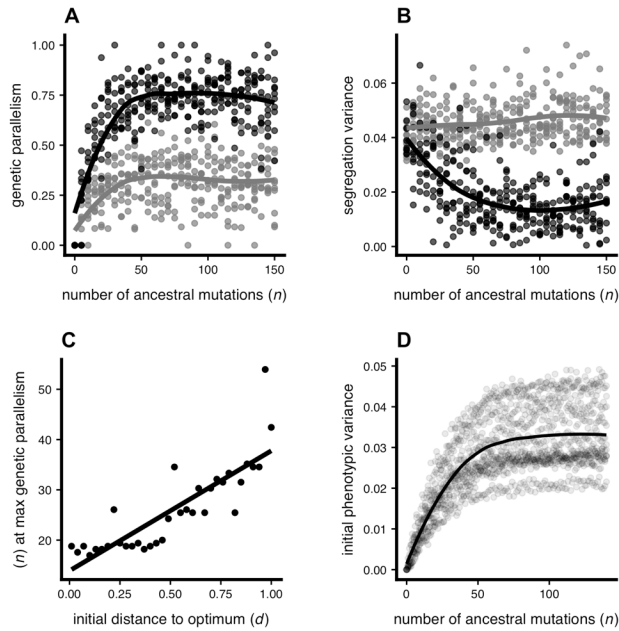
898
899
900
901
902
903
904
905
906
907
908
909
910

Figure S9. Mutation-selection balance and mutation effect sizes in ancestral populations. In panel (a) we are showing the number of segregating sites in each of 10 ancestral populations and (b) the mean frequency of the derived alleles at each of these sites in the ancestral populations. The black line is plotted through the mean of all populations at each generation, and all ten burn-ins used to generate our main text results are shown. Panel (c) illustrates the distribution of mutation effect sizes—the Euclidean distance of a mutational vector in phenotypic space—at the end of a single representative burn-in simulation (dark green), as compared to the distribution of mutations that arise *de novo* (light green). The vertical lines represent the median mutation effect size for each group. Panel (d) represents the site-frequency spectrum for segregating sites (excluding sites that have fixed). And panel (e) shows the phenotypic variance in the ancestral population over time. ($m = 5$ for all simulations shown; for rest of parameters see Table 1).



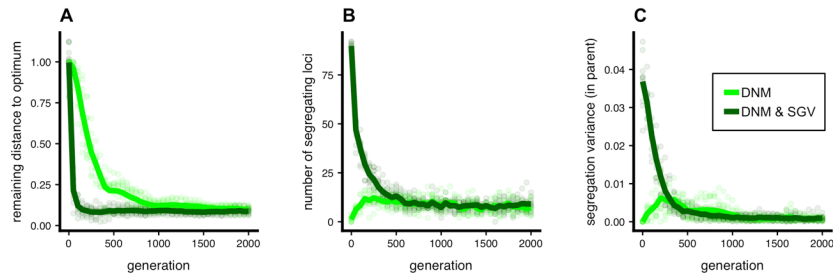


911
912 **Figure S10. Mutation-selection balance and mutation effect sizes in ancestral populations**
913 under stronger selection ($\sigma_{\text{anc}} = 1$). These parameter values imply $\mu \ll \alpha^2 \sigma$, as in the House-of-
914 Cards regime (Turelli 1984, 1985) from a Gaussian regime under the alternative set of
915 parameters.. (a) The number of segregating sites in each of 10 ancestral populations and (b) the
916 mean frequency of derived alleles at each of these sites in the ancestral populations. The black
917 line is plotted through the mean of all populations at each generation, and all ten burn-ins used to
918 generate the results ([e] and [f]) are shown. Panel (c) illustrates the distribution of mutation effect
919 sizes—the absolute value of a mutation’s effect on the phenotype—at the end of a single burn-in
920 simulation, as compared to the distribution of mutations that arise *de novo*. The vertical lines
921 represent the median mutation effect size for each group. Panel (d) represents the site-frequency
922 spectrum histogram for segregating sites. (Compare these to Fig. S1). Panels (e) and (f) are as in
923 Fig. 2A and 3B in the main text. For unspecified parameters see Table 1 in the main text. This
924 parameter combination t



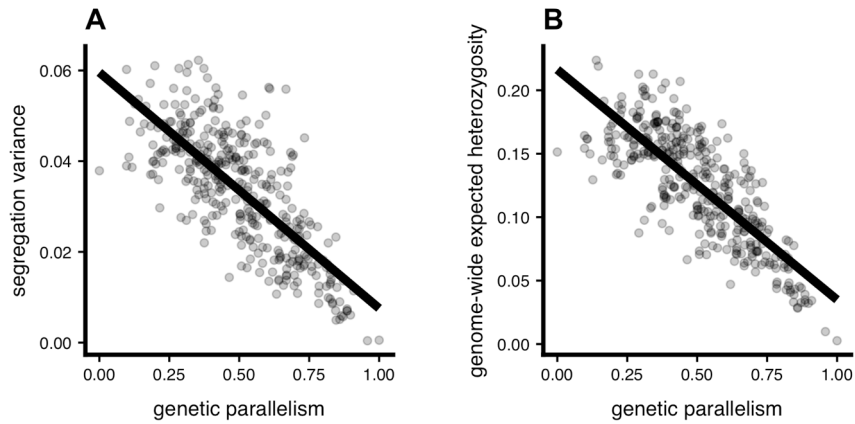
925
926
927
928
929
930
931
932
933
934
935
936
937

Figure S11. The effects of standing genetic variation on genetic parallelism and phenotypic segregation variance in hybrids under parallel and divergent natural selection. We show (a) genetic parallelism (main text equation 2) and (b) net segregation variance for populations founded with varying quantities of ancestral standing variation (n : number of ancestral mutations). Populations were subject to either parallel ($\theta = 0^\circ$; black) and divergent ($\theta = 180^\circ$; grey) selection, with $d=1$, and there were 10 replicate simulations per parameter combination. Genetic parallelism values of 0 indicate no parallelism and values of 1 indicate complete parallelism (main text Eq. 2). The curves are loess fits. Panel (c) shows that the quantity of ancestral standing variation that maximizes genetic parallelism under parallel selection ($\theta = 0^\circ$) increases when populations adapt to more distant optima. A value of $d = 1$ is 10 mutational SDs. The line is a linear regression. Panel (d) shows the relationship between the genetic (phenotypic) variation in a parental population as a function of n .

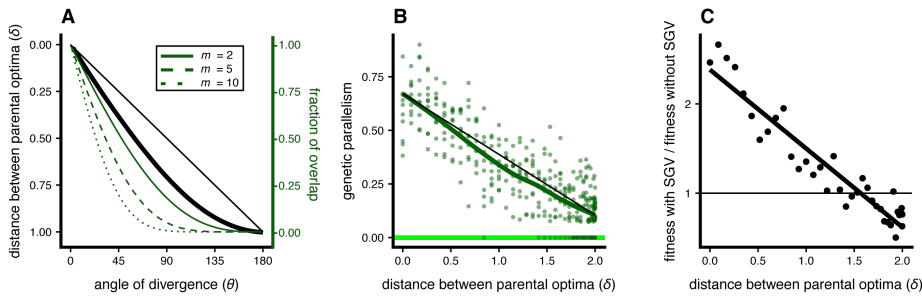


938
939
940
941
942
943
944
945
946
947
948
949
950

Figure S12. Effect of standing variation on the pace of adaptation and attainment of mutation-selection-drift balance. (a) Populations that adapt with standing variation in addition to new mutation (DNM & SGV; $n = 100$ segregating alleles; dark green) reach the phenotypic optimum more quickly than populations that adapt from new mutation only (DNM; $n = 0$ segregating alleles; light green). (b) Although populations equipped with standing variation adapt more quickly than populations adapting from new mutation only, they both reach mutation-selection-drift balance by generation 2000. (c) The phenotypic (genotypic) variance in parental populations, calculated as it is in hybrids (see main text), is stable and near zero by the end of each simulation. The initial distance to the optima, d , is 1 for all simulations. We plot 10 replicate simulations, and lines connect the mean values at each sampled generation. For unspecified parameters see Table 1 in the main text.

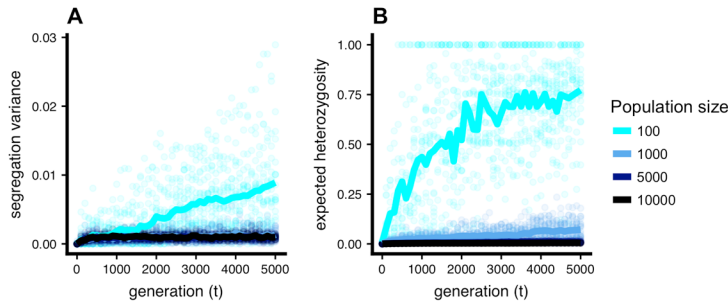


951
952 **Figure S13. Relationship between genetic parallelism and (a) segregation variance and (b)**
953 **expected heterozygosity.** Our metric of genetic parallelism (main text equation 2) is on the x-
954 axis. This is the data plotted in Fig. 2A & 2C of the main text. We show the correlation between
955 genetic parallelism and (a) segregation variance ($r^2 = 0.56$) and (b) genome-wide expected
956 heterozygosity ($2p[1-p]$, averaged across all loci ($r^2 = 0.63$). Patterns were similar for F_{ST} (Hudson
957 et al. 1992) and net π (Nei and Li 1979) (not shown).

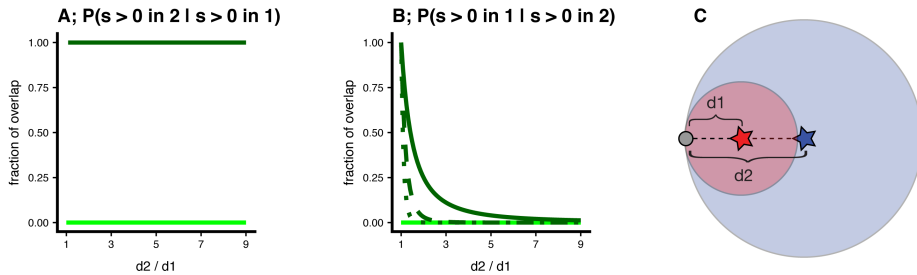


958
959
960
961
962
963
964
965
966
967
968
969
970

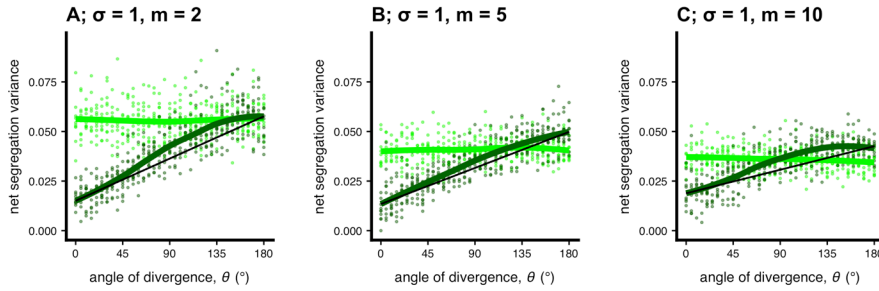
Figure S14. Alternative presentation of simulation results across environments: distance between optima (δ). Panel (a) plots the relationship between the angle of divergence, θ , and the Euclidean distance between parental optima, δ (thick black line; note reversal of y-axis; scaled between 0 and 1 by dividing by $2d$). We also plot the fraction of non-overlap as in the main text Fig. 2B (thin dark green lines; $m = 2, 5, 10$ in increasing steepness). Panel (b) shows genetic parallelism vs. δ . For a given value of θ , δ is invariant with dimensionality (i.e., the distance between optima does not change as dimensionality increases). Accordingly, the nonlinearity emerges even when considering δ , but only appreciably when considering higher dimensions ($m > 5$). In both panels, the thin and straight black line connects the fit at 0° with 180° for visual reference. In panel (c) we show the results for hybrid fitness, similar to Fig. 3B in the main text. All panels show simulations conducted in 10 dimensions ($m = 10$, $\sigma = 1$, $N = 1000$).



971
972 **Figure S15. The effect of population size on the rate of divergence between populations due**
973 **to drift.** We show populations held at a common optimum with no standing variation (i.e. $d = 0$,
974 $n = 0$) and plot (a) segregation variance and (b) expected heterozygosity in hybrids over time for
975 5,000 generations. The evolution of segregation variance is proportional to the rate of evolution
976 of reproductive isolation under parallel natural selection. Greater drift in smaller populations
977 leads to greater segregation variance and heterozygosity. The lines are drawn as the average of
978 10 replicate simulations ($m = 5$, $\sigma = 1$).



979
980 **Figure S16. Fraction of overlap of beneficial mutations with parallel selection ($\theta = 0^\circ$) but**
981 **unequal distance ($d_1 \neq d_2$).** The main text explores how the fraction of overlap changes with
982 theta while holding $d_1 = d_2 = d$ constant. Here we explore how the fraction of overlap changes
983 with the ratio d_2/d_1 when holding $\theta = 0^\circ$ constant. Unlike the metric presented in the main text
984 this metric is asymmetrical because one population is completely contained within the other.
985 Panel (A) plots the fraction of overlap for population 1 (the fraction of alleles that are beneficial
986 in population 1 are also beneficial in population 2) as a function of d_2/d_1 . With $d_1 < d_2$ the value
987 is 1 for any ratio d_2/d_1 because population 1's hypersphere is contained within population 2's.
988 Panel (B) plots the fraction of alleles that are beneficial in population 2 that are also beneficial in
989 population 1. This latter result mirrors what is seen in the main text Fig. 3C: as the locations of
990 the optima depart from one another the fraction of overlap rapidly approaches zero and does so
991 most rapidly at the onset of departure. Panel (C) shows an cartoon example of a case in 2D
992 where $d_2 = 2d_1$.
993



994
995
996
997
998
999
1000
1001

Figure S17. Effect of dimensionality on net segregation variance per dimension. The average segregation variance for a given dimension declines with dimensionality. These plots are similar to Fig. 2C in the main text except we show results for three different dimensionalities. Under divergent natural selection, simulations where populations adapted from standing variation had higher segregation variance—relative to simulations where populations adapted only from *de novo* mutation—in higher dimensions.

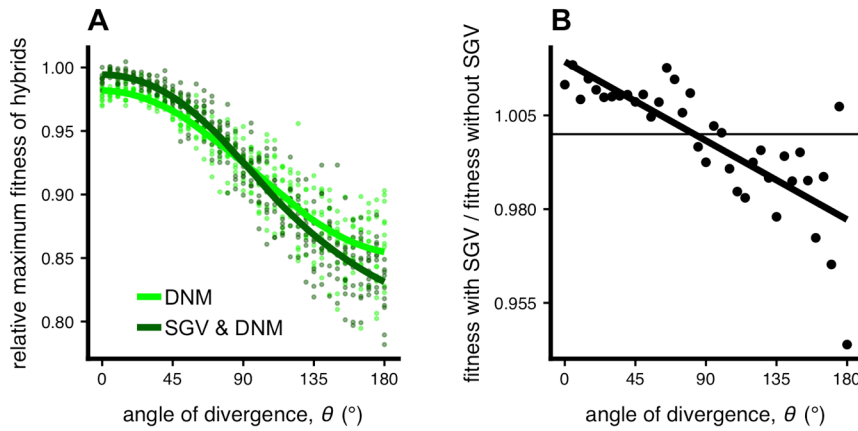
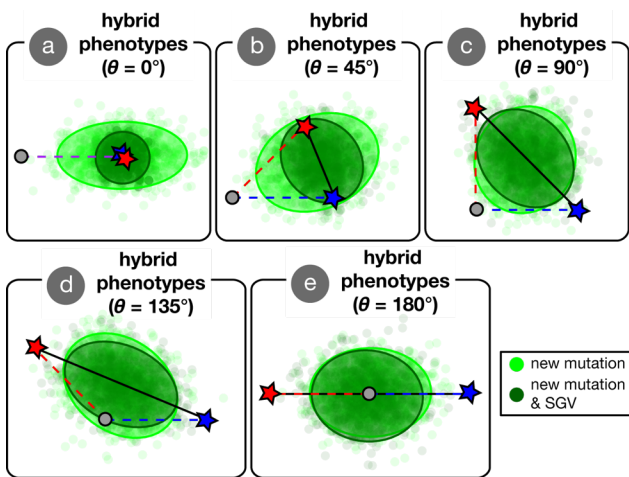
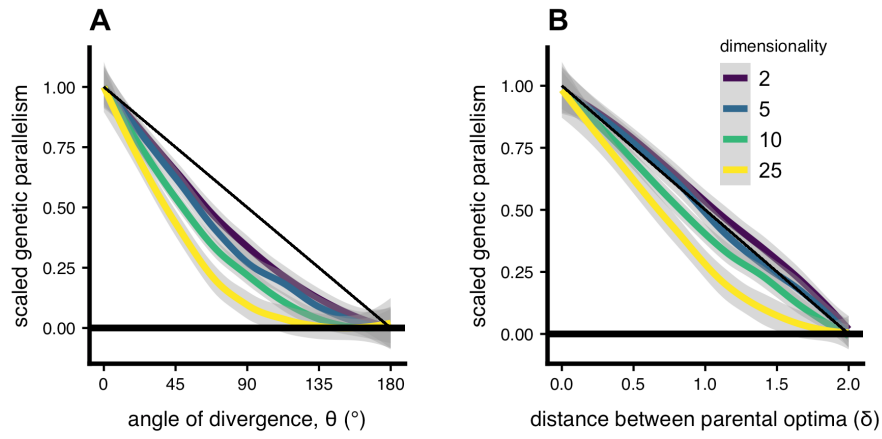


Figure S18. The effect of standing genetic variation (SGV) on relative maximum hybrid fitness across environments. Data are from simulations plotted in the main text, but instead of mean fitness of all hybrids we depict the mean fitness of the top 5 % of hybrids relative to the mean fitness of parents. We plot both the (a) raw values of relative maximum fitness and (b) the effect of standing variation on maximum hybrid fitness (dark green divided by light green).



1009
1010 **FIGURE X. The effect of standing variation on the distribution of hybrid phenotypes.** This plot
1011 We plot hybrid phenotypes (points) and 95 % confidence ellipses for five angles of divergence
1012 (**THETA**) evenly spaced along the continuum of (a) completely parallel (0°) to completely (e)
1013 divergent (180°) for simulations where populations adapted from only new mutation (light
1014 green) or both new mutation and standing genetic variation (dark green; 1000 hybrids each
1015 from ten replicate simulations each producing 100 hybrids). Parental optima are depicted as
1016 stars and the origin (ancestral optimum) is shown as a grey dot. The axes of selection connect
1017 the origin and optima (dashed red and blue lines) and we also show the axis connecting
1018 parental optima as a black line. We show the first two (of five) phenotypic dimensions, which
1019 are the only dimensions in which the optima might differ.
1020



1021
1022 **FIGURE SX. Depiction of simulation results for genetic parallelism on the same scale.** We plot
1023 four dimensionalities, and compare genetic parallelism—scaled between 1 (maximum value of
1024 loess fit) and 0 (minimum value of loess fit).

1025

1026